ON COMPUTING MULTIPLE SOLUTIONS OF NONLINEAR PDES WITHOUT VARIATIONAL STRUCTURE

A Dissertation

by

CHANGCHUN WANG

Submitted to the Office of Graduate Studies of
Texas A&M University
in partial fulfillment of the requirements for the degree of

DOCTOR OF PHILOSOPHY

May 2012

Major Subject: Mathematics

ON COMPUTING MULTIPLE SOLUTIONS OF NONLINEAR PDES WITHOUT VARIATIONAL STRUCTURE

A Dissertation

by

CHANGCHUN WANG

Submitted to the Office of Graduate Studies of
Texas A&M University
in partial fulfillment of the requirements for the degree of

DOCTOR OF PHILOSOPHY

Approved by:

Chair of Committee,	Jianxin Zhou
Committee Members,	Jay Walton
	Goong Chen
	Siu A. Chin
	Raytcho Lazarov
Head of Department,	Emil Straube

May 2012

Major Subject: Mathematics

ABSTRACT

On Computing Multiple Solutions of Nonlinear PDEs without Variational Structure. (May 2012)
Changchun Wang, B.S.; M.S., Shanghai University
Chair of Advisory Committee: Dr. Jianxin Zhou

Variational structure plays an important role in critical point theory and methods. However many differential problems are non-variational i.e. they are not the Euler-Lagrange equations of any variational functionals, which makes traditional critical point approach not applicable. In this thesis, two types of non-variational problems, a nonlinear eigen solution problem and a non-variational semi-linear elliptic system, are studied.

By considering nonlinear eigen problems on their variational energy profiles and using the implicit function theorem, an implicit minimax method is developed for numerically finding eigen solutions of focusing nonlinear Schrödinger equations subject to zero Dirichlet/Neumann boundary condition in the order of their eigenvalues. Its mathematical justification and some related properties, such as solution intensity preserving, bifurcation identification, etc., are established, which show some significant advantages of the new method over the usual ones in the literature. A new orthogonal subspace minimization method is also developed for finding multiple (eigen) solutions to defocusing nonlinear Schrödinger equations with certain symmetries. Numerical results are presented to illustrate these methods.

A new joint local min orthogonal method is developed for finding multiple solutions of a non-variational semi-linear elliptic system. Mathematical justification and convergence of the method are discussed. A modified non-variational Gross-Pitaevskii system is used in numerical experiment to test the method.

ACKNOWLEDGMENTS

Foremost I would like to thank my thesis advisor, Dr. Jianxin Zhou, for his encouragement and guidance during my graduate study and in the preparations of this thesis. Particularly, I thank him for choosing an challenging while interesting topic that fits my background very well. I also thank him for partially support my research with his NSF grant under DMS-0713872/0820327/1115384.

I would also thank the member of my advisory committee, Dr. Jay Walton, Dr. Goong Chen, Dr. Siu A. Chin and Dr. Raytcho Lazarov for their service on my oral examinations and their useful comments, questions and advices on my thesis.

I would like to express my gratitude to Ms. Monique Stewart for her incredible patience and knowledge with the university administration. I also thank the students in the mathematics department, specifically Dr. Xianjin Chen, Dr. Yan li, and Jia Wei for their kindness.

NOMENCLATURE

ESP	eigen solution problem
JLMOM	joint local min-orthogonal method
LMM	local min-max method
LMOM	local min-orthogonal method
MI	Morse index
MSIS	maximum symmetry invariant subspace
NLS	nonlinear Schrödinger equation
NVS	non-variational system
PDE	partial differential equation
RRM	Rayleigh-Ritz method

TABLE OF CONTENTS

Page

Page

LIST OF TABLES

LIST OF FIGURES

FIGURE Page

FIGURE Page

1. INTRODUCTION

1.1 Non-variational Problems and Their Difficulties

Calculus of variations provides a strong connection between partial differential equations(PDE) and critical point theory[21]. A PDE is *variational* if it is the Euler-Lagrange equation $J'(u) = 0$ of a Frechet differentiable functional $J(u)$. A point u^* is called a critical point of J if $J'(u^*) = 0$. So solutions to PDE correspond to the critical points of their variational functionals.

For example, the nonlinear boundary value problem

$$\begin{cases} -\nabla \cdot \nabla u(x) + f(u(x), x) = 0 & x \in \Omega, \\ \dfrac{\partial u(x)}{\partial n} + cu(x) + g(x) = 0 & x \in \partial\Omega, \end{cases} \tag{1.1}$$

can be solved by finding the critical points of its variational functional

$$J(u(x)) = \int_\Omega [\frac{1}{2}|\nabla u(x)|^2 + F(u(x), x)]dx + \int_{\partial\Omega} [\frac{1}{2}cu^2(x) + g(x)u(x)]ds \tag{1.2}$$

where $F_u(u(x), x) = f(u(x), x)$. Actually, for any function v

$$\begin{aligned} J'(u)(v) &= \frac{dJ(u+tv)}{dt}|_{t=0} \\ &= \frac{d}{dt}[\int_\Omega [\frac{1}{2}|\nabla(u(x)+tv(x))|^2 + F(u(x)+tv(x), x)]dx \\ &\quad + \int_{\partial\Omega} [\frac{1}{2}c(u(x)+tv(x))^2 + g(x)(u(x)+tv(x))]d\sigma]|_{t=0} \\ &= \int_\Omega [\nabla v(x) \cdot \nabla u(x) + f(u(x), x)v(x)]dx + \int_{\partial\Omega} [cu(x) + g(x)]v(x)d\sigma \\ &= \int_\Omega [-\Delta u(x) + f(u(x), x)]v(x)dx + \int_{\partial\Omega} [\frac{\partial u(x)}{\partial n} + cu(x) + g(x)]v(x)d\sigma. \end{aligned}$$

This implies the equivalence $J'(u) = 0 \Leftrightarrow$ (1.1)

This dissertation follows the style of *Mathematics of Computation*.

Another example is the Sturm-Liouville problem (a linear eigen solution problem)

$$\begin{cases} -\nabla\cdot(p(x)\nabla u(x)) - q(x)u(x) = \lambda r(x)u(x)x & \in \Omega, \\ p(x)\dfrac{\partial u}{\partial n} + cu(x) = 0x & \in \partial\Omega. \end{cases} \tag{1.3}$$

where c is some constant and $p(x), q(x), r(x)$ are some positive weight functions. The variational functional (Rayleigh quotient) is

$$\lambda = \frac{Q(u)}{R(u)} \tag{1.4}$$

where

$$\begin{cases} Q(u) = & \displaystyle\int_\Omega [p(x)|\nabla u(x)|^2 - q(x)u^2(x)]dx + \int_{\partial\Omega} cu^2(x)ds, \\ R(u) = & \displaystyle\int_\Omega r(x)u^2(x)dx. \end{cases} \tag{1.5}$$

Thus,

$$\begin{aligned} [\frac{Q(u)}{R(u)}]'(v) &= \frac{Q'(u)R(u) + Q(u)R'(u)}{R^2(u)}(v) \\ &= \frac{1}{R(u)}[Q'(u) + \lambda R'(u)](v) \\ &= \frac{2}{R(u)}(\int_\Omega [(-\nabla\cdot(p(x)\nabla u(x)) - q(x)u(x) + \lambda r(x)u(x))v(x)]dx \\ &\quad + \int_{\partial\Omega}[(p(x)\frac{\partial u(x)}{\partial n} + cu(x))v(x)]ds). \end{aligned} \tag{1.6}$$

Since $R(u)$ is positive, $[\frac{Q(u)}{R(u)}]' = 0$ is equivalent to (1.3).

The variational structure plays an important role in solving PDE with multiple solutions. While classical calculus of variational focuses on finding local maximum or minimum, many PDE especially of nonlinear type have multiple solutions corresponding to saddle types i.e. critical points with both increasing and decreasing directions thus not maximum or minimum. To compute these multiple solutions,

an order of the solutions becomes very important. E.g., we can order the solutions in their Morse indices(MI) [17,16] which is the number of negative eigenvalues of the second derivative of the functional at the solutions. With the order one may discuss what new solutions are expected and whether there are solutions missing. For variational problems, we can use local min-max method developed in [11,12] to numerically compute the multiple solutions in the order of their MI.

However many PDE in application are not the Euler-Lagrange equation of any variational functional thus called *non-variational*. In this dissertation two non-variational problems are studied. New methods will be developed to compute their multiple solutions in an order.

1.2 A Semi-linear Elliptic Eigen-solution Problem

First, we discuss a nonlinear eigen solution problem. The basic model for our analysis and computation is the nonlinear Schrödinger equation (NLS). It is the equation of motion to replace Newton's 2nd law as in classical mechanics.

$$i\frac{\partial w(x,t)}{\partial t} = -\Delta w(x,t) + v(x)w(x,t) - \kappa f(x,|w(x,t)|)w(x,t), \tag{1.7}$$

$$\frac{d}{dt}\int |w(x,t)|^2 dx = 0, \tag{1.8}$$

where (1.8) represents the time-invariance condition of a wave intensity, under which NLS is derived [2] and solutions are physically meaningful, $v(x) \geq 0$ is a potential function, which in some cases traps the solutions in a local area, and κ is a physical parameter. $\kappa > 0$ corresponds to a focusing or attractive nonlinearity. $\kappa < 0$ corresponds to a defocusing or repulsive nonlinearity. e.g., the well known Gross-Pitaevskii equation in Bose-Einstein condensate is of a defocusing type NLS. Despite this minor difference in the form, those two cases are very different physically and mathematically, so we have to develop two very different methods to solve them.

To study solution pattern formation, (in)stability and other properties, standing (solitary) wave solutions of the form $w(x,t) = u(x)e^{-i\lambda t}$ are interested where λ is a *wave frequency* and $u(x)$ is a *wave amplitude function*. It leads to solve an eigen solution problem (ESP): find $(u,\lambda) \in H^1(\Omega) \times \mathbb{R}$ s.t.

$$\lambda u(x) = -\Delta u(x) + v(x)u(x) - \kappa f(x,|u(x)|)u(x). \tag{1.9}$$

Numerically (1.9) can be solved on an open bounded domain $\Omega \subset \mathbb{R}^n$ with a zero Dirichlet or Neumann (for other applications) boundary condition (B.C.).

Many research papers, e.g. [1], in the literature on studying NLS assume a normalization condition $\int_\Omega |w(x,t)|^2 dx = 1$, since the original linear Schrödinger equation is derived under this normalization condition which is, in the term of quantum physics, interpreted as the probability of w taking place. So only solutions satisfying this normalization condition are physically meaningful. However, in [2] the author derived NLS under the conservation condition (1.8) which is clearly more general than the normalization condition, and states that the normalization condition is not necessary. In particular, a standing (solitary) wave solution always satisfies the conservation condition, so there is no need to enforce the normalization condition. On the other hand, ESP (1.9) may also arise from other applications where such a normalization is not necessary. Thus in this dissertation we try to provide other options rather than such a normalization assumption.

The variational "energy" functional of (1.9) at each (u,λ) is

$$J(u,\lambda) = \int_\Omega [\frac{1}{2}(|\nabla u(x)|^2 + v(x)u^2(x) - \lambda u^2(x)) - F(x,u(x))]dx \tag{1.10}$$

where $F_u(x,u) = f(x,|u|)u$ satisfies certain regularity and growth condition. Then (u,λ) is an eigen solution to (1.9) if and only if it solves the PDE

$$J'_u(u,\lambda) = 0. \tag{1.11}$$

Note that under certain condition on $v(x)$, (1.9) has at least one solution $u \neq 0$ for each $\lambda > 0$, the problem has a one-degree freedom. So to formulate a discrete spectrum problem, one needs a scalar equation as a constraint. To find a better formulation to do so, let us observe (1.9), we can see that the nonlinearity of the problem is at the variable u not at λ. So we adopt a frequently used formulation in the literature, i.e., we denote

$$H(u) = \int_\Omega [\frac{1}{2}(|\nabla u(x)|^2 + v(x)u^2(x) - F(x, u(x))]dx \tag{1.12}$$

which is sometimes called the Hamiltonian of the wave u or the energy of u and

$$I(u) = \int_\Omega u^2(x)dx = \|u\|^2_{L^2(\Omega)} \tag{1.13}$$

which represents the intensity of the wave u in L^2-norm. Then (1.11) becomes a typical ESP

$$H'(u) = \lambda I'(u). \tag{1.14}$$

But the problem is not variational and has a one-degree freedom. In order to remove this one-degree freedom to form a discrete spectrum problem, an easy choice as suggested in [24,36] and frequently used in the literature is to assume a *level-set* constraint $I(u) = C$. Then its Lagrange functional is

$$\mathcal{L}(u, \lambda) = H(u) - \lambda(I(u) - C).$$

The problem becomes variational and is to solve for (u, λ) s.t.

$$\mathcal{L}'(u, \lambda) = (\mathcal{L}'_u(u, \lambda), \mathcal{L}'_\lambda(u, \lambda)) = (H'(u) - \lambda I'(u), C - I(u)) = (0, 0).$$

However our numerical experience in [34, 35] indicates that to put u and λ together as a variable (u, λ) of a *Lagrange functional* may not be a good idea. It causes troubles in selecting initial guesses (u_0, λ_0) for computing multiple eigen solutions and also in functional structure (mountain pass or linking) and solution instability analysis. For our model problem, the level set constraint $I(u) = C$ implies that the intensity of the eigenfunction u in L^2-norm is a constant, which may not be necessary [2]. In this paper we develop a new formulation to solve the problem rather than using the level set constraint. Also for an ESP, it is important to find solutions in an order. So one can discuss what is found or missing in a computation process. Since the eigenvalues form the best order in analysis and application of ESP, *people always want to find eigen solutions in the order of their eigenvalues.* But the Lagrange functional method or Newton iterate based methods [29] failed to do so.

An ESP $H'(u) = \lambda I'(u)$ is said to be *homogenous* if $H(tu) = t^{k+1}H(u),\ I(tu) = t^{l+1}I(u)$ for some $k, l > 0$. An ESP is said to be *iso-homogenous* if it is homogenous with $k = l$. When an ESP is iso-homogenous, different scalings yield the same eigen solution set. A Rayleigh quotient $\mathcal{R}(u) = \lambda(u) = H(u)/I(u)$ can be used in LMM ([34]) to numerically find critical points u of $\mathcal{R} = \lambda$. It is obvious that a linear ESP $J'_u(u, \lambda) = Au - \lambda Bu$ is of iso-homogeneous and a non iso-homogenous ESP yields different solution sets in different scalings. So one can see that many nice properties that a linear ESP enjoys get lost, see Table 1.1.

Our approach is to put the constraint on its variational energy profile, and then use the implicit function theorem to implicitly define the eigenvalue λ as a functional of the eigen-function u. We show that the solutions of the ESP are the critical points of the functional λ, and by applying the local min-max method, an ordered solution set can be computed.

Table 1.1
The difference between linear ESP and nonlinear ESP

Property	Linear ESP	Nonlinear ESP
different normalizations/scalings yields the same solution set	yes (iso-hom.)	no (non-iso-hom.)
a linear combination of eigenfunctions of an eigenvalue is also an eigenfunction	yes	no
eigenfunctions of different eigenvalues are orthogonal	yes	no
eigenfunctions form a basis	yes	no

1.3 A Semi-linear Elliptic System without a Common Variational Form

Next, we discuss a semi-linear non-variational elliptic system, another type non-variational problem. Consider the following elliptic system

$$\begin{cases} -\Delta u(x) + f(x, u(x), v(x)) = 0, \\ -\Delta v(x) + g(x, u(x), v(x)) = 0, \end{cases} \tag{1.15}$$

for $x \in \Omega$ and satisfy zero Dirichlet B.C. For each equation of the system we can denote its variational functional with respect to one variable in the following form

$$\begin{aligned} F(u(x), v(x)) &= \bar{F}(u(x)) + W^1(u(x), v(x)), \\ G(u(x), v(x)) &= \bar{G}(v(x)) + W^2(u(x), v(x)), \end{aligned} \tag{1.16}$$

with

$$\begin{aligned} F_u(u(x), v(x)) &= -\Delta u(x) + f(x, u(x), v(x)), \\ G_v(u(x), v(x)) &= -\Delta v(x) + g(x, u(x), v(x)), \end{aligned}$$

where $W^1(u(x), v(x))$ and $W^2(u(x), v(x))$ contain only interaction terms of $u(x)$ and $v(x)$ and play an important role on whether the problem is variational or not. When $W^1(u(x), v(x)) = k \cdot W^2(u(x), v(x))$, $k \in \mathbb{R}^+$, the system is *variational cooperative*[42], i.e., $\exists J(u(x), v(x)) = k \cdot \bar{F}(u(x)) + k \cdot W^1(u(x), v(x)) + \bar{G}(v(x))$ s.t.

$$\begin{cases} J_u(u(x), v(x)) = & k \cdot F_u(u(x), v(x)) = -\Delta u(x) + f(x, u(x), v(x)) = 0, \\ J_v(u(x), v(x)) = & G_v(u(x), v(x)) = -\Delta v(x) + g(x, u(x), v(x)) = 0. \end{cases} \tag{1.17}$$

When $W^1(u(x), v(x)) = -k \cdot W^2(u(x), v(x))$, $k \in \mathbb{R}^+$, the system is *variational non-cooperative* [40], i.e., $\exists J(u(x), v(x)) = k \cdot \bar{F}(u(x)) + k \cdot W^1(u(x), v(x)) - \bar{G}(v(x))$ s.t.

$$\begin{cases} J_u(u(x), v(x)) = & k \cdot F_u(u(x), v(x)) = -\Delta u(x) + f(x, u(x), v(x)) = 0, \\ J_v(u(x), v(x)) = & -G_v(u(x), v(x)) = \Delta v(x) - g(x, u(x), v(x)) = 0. \end{cases} \tag{1.18}$$

But when $W^1(u(x), v(x))$ and $W^2(u(x), v(x))$ are not proportional, there is no common $J(u(x), v(x))$ s.t. its Euler-Lagrange equation $(J_u(u(x), v(x)), J_v(u(x), v(x))) = (0, 0)$ is the original system, and thus the system is *non-variational*.

1.4 A Survey of Existing Numerical Methods Dealing with Nonlinear Elliptic PDEs.

In this section, we briefly introduce some existing numerical methods which are applicable to nonlinear elliptic PDEs. Their advantage and disadvantage will be briefly addressed.

Monotone iteration method[3,8]

For semi-linear elliptic equation

$$\begin{aligned} \Delta u(x) &= F(x, u(x)) \qquad x \in \Omega \\ B(u(x)) &= g(x) \qquad x \in \partial\Omega. \end{aligned} \tag{1.19}$$

Choose a sufficient large λ, the monotone iteration scheme is

$$\Delta u_{n+1} - \lambda u_{n+1} = -\lambda u_n + F(x, u_n). \tag{1.20}$$

A numerical method for solving linear elliptic equation such as finite element method, boundary element method or spectrum method etc. need to be implemented in each iteration to solve u_{n+1}. The method is very simple and easy to implement. However, it mainly focuses on finding stable state solutions, and is hard to capture unstable solutions. A local convergence of the algorithm is established.

The imaginary-time evolution method(ITEM)[32]

For equation

$$\begin{aligned} -\Delta u(x) + \mu u(x) - F(u^2(x), x)u(x) &= 0 \qquad x \in \Omega \\ u(x) &= 0 \qquad x \in \partial\Omega \end{aligned} \tag{1.21}$$

where $L_{00} = \Delta u + F(u^2, x)$, $P = \|u_0\|_{L_2}$. The ITEM iteration is

$$\hat{u}_{n+1} = u_n + [L_{00}u]_{u=u_n}\Delta t \tag{1.22}$$

$$u_{n+1} = \left(\frac{P}{\langle \hat{u}_{n+1}, \hat{u}_{n+1} \rangle}\right)^{\frac{1}{2}} \hat{u}^{n+1}. \tag{1.23}$$

The generalized Petviashili method[14]

Consider a more general semi-linear elliptic equation

$$L_0 u(x) = 0 \qquad x \in \Omega \tag{1.24}$$
$$u(x) = 0 \qquad x \in \partial\Omega.$$

Let L_1 be the linear approximation of L_0, s.t. $L_0 = L_1 + O(u^2)$ near u. N is a self-adjoint linear operator satisfying $L_1 u \approx \alpha N u$ and $\gamma = 1 + \frac{1}{\alpha \Delta t}$.

The Generalized Petvoashvili iteration scheme is

$$u_{n+1} - u_n = (N^{-1}(L_0 u)_n - \gamma \frac{\langle u_n, (L_0 u)_n \rangle}{\langle u_n, N u_n \rangle} u_n)\Delta t. \tag{1.25}$$

The accelerated imaginary-time evolution method(AITEM)[32]

The AITEM is actually a preconditioned ITEM method. Let M be a positive-definite and self-adjoint operator. For (1.21), the AITEM iteration is

$$u_{n+1} = (\frac{P}{\langle \hat{u}_{n+1}, \hat{u}_{n+1} \rangle})^{\frac{1}{2}} \hat{u}_{n+1} \tag{1.26}$$
$$\hat{u}_{n+1} = u_n + M^{-1}[L_{00} u - \mu]_{u=u_n, \mu=\mu_n} \Delta t \tag{1.27}$$
$$\mu_n = \frac{\langle L_{00} u, M^{-1} u \rangle}{\langle u, M^{-1} u \rangle}|_{u=u_n}. \tag{1.28}$$

Squared-operator iteration method(SOM)[14,15]

For (1.24), let $L_0 = L_1 + O(u^2)$ near u. N is the self-adjoint linear operator satisfying $L_1 u \approx \alpha N u$. M be a positive-definite and self-adjoint operator.

The SOM iteration is

$$u_{n+1} = u_n - [M^{-1} N M^{-1} L_0 u]_{u=u_n} \Delta t. \tag{1.29}$$

The ITEM type methods(Petviashili method,AITEM,SOM) require a close initial to make the methods convergent. The original ITEM can only compute ground state solutions, but some later variants of this type can capture sign-change solutions.

Newton type methods[18,19,31,4]

Newton's method is perhaps the most popular numerical scheme to solve nonlinear PDEs. Even now, various modified Newton's methods appear in newly published papers. The original Newton's method is very simple. For a non-linear boundary value problem

$$F(x, u(x)) = 0 \qquad x \in \Omega \tag{1.30}$$
$$B(u(x)) = g(x) \qquad x \in \partial\Omega.$$

The newton iteration is then

$$u_{n+1} = u_n - \alpha(n) F'^{-1}(u_n) F(u_n), \tag{1.31}$$

where $\alpha(n)$ is a step size determined by various strategies.

Newton's method, if successful, converges very fast compared to other methods, so it can be used to speed up local convergence in other methods. However Newton's method can not handel degeneracy, i.e., when F'(u) is singular, Newton's method encounters difficulty. And it also highly relies on initial guesses, which limits it to those models whose solutions are predictable.

Modified mountain pass method[5]

The modified mountain pass method is an variational method which computes the critical point with Morse index 1 of a functional J.

Step 1: Give initial guess $\hat{w}$. Let $k = 0$ and compute $w_k = arg \max_{t>0} J(tw)$;

Step 2: Compute $d_k = -\nabla J(w_k)$, if $\|d_k\| < \varepsilon$, stop and output w_k;

Step 3: Compute $w^k := arg\min_{\tau>0}\max_{t>0} J(t(w_k + \tau\hat{w}_k))$, $k = k + 1$, goto step2.

The most notable feature of this method is that it is a two-level methods, in the inner level a maximization is taken over an affine line and in the outer level a minimization is taken over all the maxima gotten from the inner level. This gives a mountain pass solution [5] or $MI = 1$.

High link method[9,23]

The high link method is also a two-level method. In the inner level a maximization is taken over a triangular region nd in the outer level a minimization is taken over all the maxima gotten from the inner level. This gives a solution [9] of $MI = 2$.

Local min-max method(LMM)[11,12]

The local min max method is a two-level optimization method develop in a series of papers to compute the multiple solutions of PDEs in the order of their MI. A support subspace is used in the method to determine the Morse index of a solution and separate new solutions from old ones. When the support subspace is set to be 0, LMM reduces to the modified mountain pass method and when the support subspace is set to be spanned by a solution of $MI = 1$ LMM reduces to the high link method. It can compute solutions with high MI, see section 2.2.1 for more details.

Local min-orthogonal method(LMOM) [40, 41, 42]

Local min-orthogonal method is developed for solving a variational elliptic system. It can compute multiple solutions of the system in an order based on the variational energies of each individual equation in the system.

Based on the above survey, it is clear that those metioneded methods are either not suitable or can not be applied directly to the problems we want to solve for multiple solutions in this dissertation and hence new approach must be developed.

2. NONLINEAR EIGEN SOLUTION PROBLEM

In this chapter we discuss the nonlinear ESP problem (1.9) of both focusing and defocusing types. A new setting of the problem on variational energy profile is adopted. The local min-max method is then applied to solve the focusing type ESP. For defocusing type problems, a new orthogonal subspace minimization method is developed to solve certain problems with symmetries. The content of this chapter is also in my two submitted papers [27,28].

2.1 A New Setting of ESP on Variational Energy Profile

Let's start our discussion from a homogenous ESP (1.12),(1.13),and (1.14). We have

$$\begin{aligned} \langle H'(u), u\rangle &= \frac{d}{ds}|_{s=0} H((1+s)u) = (k+1)H(u), \\ \langle I'(u), u\rangle &= \frac{d}{ds}|_{s=0} I((1+s)u) = (l+1)I(u). \end{aligned}$$

Then at an eigen solution pair (u, λ),

$$\langle H'(u), u\rangle = \langle \lambda I'(u), u\rangle \Rightarrow H(u) = \frac{l+1}{k+1}\lambda I(u).$$

Thus the level set constraint $I(u) = C$ is equivalent to the constraint

$$H(u) = \frac{l+1}{k+1}C\lambda \text{ or } J(u,\lambda) = H(u) - \lambda I(u) = (\frac{l+1}{k+1} - 1)C\lambda, \tag{2.1}$$

i.e., the variational energy values of J at (u, λ) are proportional to λ. The level set constraint $H(u) = C$ is equivalent to the constraint

$$H(u) = \frac{k+1}{l+1}\frac{C}{\lambda} \text{ or } J(u,\lambda) = H(u) - \lambda I(u) = (1 - \frac{k+1}{l+1})C, \tag{2.2}$$

i.e., the variational energy values of J at (u, λ) are fixed at a constant level. If ESP is iso-homogenous, $k = l$, the above reduces to $J(u, \lambda) = 0$ and becomes the Rayleigh quotient method $\lambda(u) = \frac{H(u)}{I(u)}$. However the above equivalences broken for non-iso-homogenous ESP and those constraints will lead to different eigen solution sets. Non-homogenous EPS with level set constraint is studied in [35].

Assume $I(u) > 0, u \neq 0$ as in many applications. Let C be a $\mathcal{C}^2$ function s.t. $C'(\lambda) \geq 0$ (i.e. J is increasing in λ) and for each $u \neq 0$, there is unique λ s.t. $J(u, \lambda) = H(u) - \lambda I(u) = C(\lambda)$. By the implicit function theorem, a functional $\lambda(u)$ can be implicitly defined from

$$J(u, \lambda(u)) = H(u) - \lambda(u) I(u) = C(\lambda(u))$$

with

$$\lambda'(u) = [I(u) + C'(\lambda(u))]^{-1}[H'(u) - \lambda(u) I'(u)].$$

Since $I(u) + C'(\lambda(u)) > 0$, we have

$$\lambda'(u) = 0 \Leftrightarrow H'(u) = \lambda I'(u). \tag{2.3}$$

We need some notions from critical point theory. Let $\lambda : H \to \mathbb{R}$ be a $\mathcal{C}^2$ functional. A point $u^* \in H$ is said to be a critical point of λ if $\lambda'(u^*) = 0$. Let $H = H^+ \oplus H^0 \oplus H^-$ be the spectrum decomposition of the linear operator $\lambda''(u^*)$, i.e. H^+, H^0, H^- are respectively the maximum positive, the null and the maximum negative subspaces of $\lambda''(u^*)$. u^* is said to be *nondegenerate* if $H^0 = \{0\}$. Otherwise u^* is said to be *degenerate* and $\dim(H^0)$ is called the nullity of u^*. $\dim(H^-)$ is the Morse index as we mentioned in introduction and denoted by $\mathrm{MI}(u^*)$ at the critical point u^*, which measures the instability of u^*, an important information in system design/control and bifurcation analysis.

2.2 Application to Focusing Schrödinger ESP

Let $v = 0$ and $F(x, u(x)) = \frac{|u(x)|^{p+1}}{p+1}$ in (1.10) subject to either zero Dirichlet or Neumann B.C. where $1 < p < p^*$ and p^* is the critical Sobolev exponent [22], i.e., we solve ESP

$$-\Delta u(x) - |u(x)|^{p-1}u(x) = \lambda u(x) \tag{2.4}$$

and set

$$J(u,\lambda) = H(u) - \lambda I(u) = \int_\Omega [\frac{1}{2}|u(x)|^2 - \frac{1}{2}\lambda u^2(x) - \frac{1}{p+1}|u(x)|^{p+1}]dx = C(\lambda) \tag{2.5}$$

where

$$H(u) = \int_\Omega [\frac{1}{2}|\nabla u(x)|^2 - \frac{1}{p+1}|u(x)|^{p+1}]dx \quad \text{and} \quad I(u) = \int_\Omega \frac{1}{2}u^2(x)dx.$$

Multiplying (2.4) by u and integrating on Ω give

$$\int_\Omega [|\nabla u(x)|^2 - \lambda u^2(x) - |u(x)|^{p+1}]dx = 0. \tag{2.6}$$

Taking (2.5) into account, for any eigenfunction u, we obtain

$$C(\lambda) = [\frac{1}{2} - \frac{1}{p+1}] \int_\Omega |u(x)|^{p+1}dx > 0. \tag{2.7}$$

So we must have $C(\lambda) > 0$ and $C'(\lambda) \geq 0$.

(1) When $C(\lambda) = C$, we must have $C > 0$ and

$$\|u\|^{p+1}_{L^{p+1}} = \frac{2(p+1)}{p-1}C. \tag{2.8}$$

for any eigenfunction u. By the Holder inequality, there exists $C_p > 0$ s.t.

$$\|u\|_{L^2} < C_p. \tag{2.9}$$

Theorem 2.2.1 *Let $u_k, k = 1, 2, ...$ be all the eigenfunctions. Then $\|u_k\|^{p+1}_{L^{p+1}} = C_1$ for some constant $C_1 > 0$ if and only if $J(u_k) = H(u_k) - \lambda(u_k)I(u_k) = C_2$ for some constant $C_2 > 0$.*

Proof By (2.8), we only have to show the "only if" part. When $\|u_k\|^{p+1}_{L^{p+1}} = C_1 > 0$, we have

$$J(u_k) = H(u_k) - \lambda(u_k)I(u_k) = \frac{1}{2}\|\nabla u_k\|^2_{L^2} - \frac{1}{p+1}C_1 - \frac{1}{2}\lambda(u_k)I(u_k).$$

(2.6) gives

$$\|\nabla u_k\|^2_{L^2} - \lambda(u_k)I(u_k) = \|u_k\|^{p+1}_{L^{p+1}} = C_1.$$

Thus

$$J(u_k) = \frac{1}{2}C_1 - \frac{1}{p+1}C_1 = (\frac{1}{2} - \frac{1}{p+1})C_1,$$

i.e., $C_2 = (\frac{1}{2} - \frac{1}{p+1})C_1 > 0$. ■

Remark 2.2.1 *Note that $\|u_k\|_{L^2}$ and $\|u_k\|_{L^{p+1}}$ measure the intensity of u_k in two different norms. When $\|u_k\|_{L^2} = C > 0$ is usually used as a constraint in the literature, there is no control over the intensity $\|u_k\|_{L^{p+1}}$; when we use $\|u_k\|_{L^{p+1}} = C$ as a constraint, the intensity $\|u_k\|_{L^2}$ is also well-under control. This shows a significant advantage of our approach over the usual ones in the literature.*

(2) When $C(\lambda) = C\lambda$ we must have $C > 0, \lambda > 0$, (2.7) becomes

$$\|u\|^{p+1}_{L^{p+1}} = \frac{2(p+1)}{p-1}C\lambda. \tag{2.10}$$

Plugging (2.10) into (2.5), we obtain

$$\frac{1}{2}\|\nabla u\|_{L^2}^2 - \frac{\lambda}{2}\|u\|_{L^2}^2 - \frac{2C\lambda}{p-1} = C\lambda \quad \text{or} \quad \frac{1}{2}\|\nabla u\|_{L^2}^2 = \lambda(\frac{1}{2}\|u\|_{L^2}^2 + \frac{p+1}{p-1}C).$$

Since $\lambda(u)$ is derived from our new formulation and different from the usual ones in the literature, we need to know some of its basic properties. For example, for LMM to work on, one needs that for each $u \neq 0$, $\lambda(tu)$ attains its local maximum at certain $t_u > 0$ and $\lim_{t\to+\infty} \lambda(tu) = -\infty$. Such a structure is usually called a mountain-pass structure, which is motivated by the wellknown mountain pass lemma [22]. Typically in the mountain pass lemma, a variational functional needs to be $\mathcal{C}^1$.

(1) When $C(\lambda) = C > 0$, we have

$$\lambda'(u) = [I(u)]^{-1}[H'(u) - \lambda(u)I'(u)]$$

where $I(u) + C'(\lambda(u)) = I(u) > 0$ for all $u \neq 0$ and

$$\lambda(u) = [I(u)]^{-1}[H(u) - C] = [\int_\Omega \frac{1}{2}u^2(x)dx]^{-1} \int_\Omega [\frac{1}{2}|\nabla u(x)|^2 - \frac{|u(x)|^{p+1}}{p+1}]dx - C.$$

Thus

$$\lim_{t\to 0^+} \lambda(tu) = -\infty, \ \lim_{t\to+\infty} \lambda(tu) = -\infty.$$

It is clear that $\lambda(u)$ has a singularity at $u = 0$. But $u = 0$ is not an eigenfunction, thus we still call such a structure a mountain-pass type structure with a singularity at $u = 0$.

(2) When $C(\lambda) = C\lambda$ with $C > 0$, we have

$$\lambda'(u) = [I(u) + C]^{-1}(H'(u) - \lambda(u)I'(u)),$$

$$\lambda(u) = [I(u) + C]^{-1}H(u) = [\int_\Omega \frac{1}{2}u^2(x)dx + C]^{-1}\Big(\int_\Omega [\frac{1}{2}|\nabla u(x)|^2 - \frac{|u(x)|^{p+1}}{p+1}]dx\Big).$$

Thus

$$\lim_{t\to 0^+} \lambda(tu) = 0^+, \ \lim_{t\to+\infty} \lambda(tu) = -\infty.$$

It also shows a typical mountain pass structure. In either case, see Fig. 2.1, for each $u \neq 0$, there exists $t_u > 0$ s.t.

$$t_u = \arg\max_{t>0} \lambda(tu) \quad \text{or} \quad \frac{d}{dt}\lambda(tu)|_{t=t_u} = \langle \lambda'(t_u u), u\rangle = 0. \tag{2.11}$$

So we can expect to use LMM to numerically find critical points of λ.

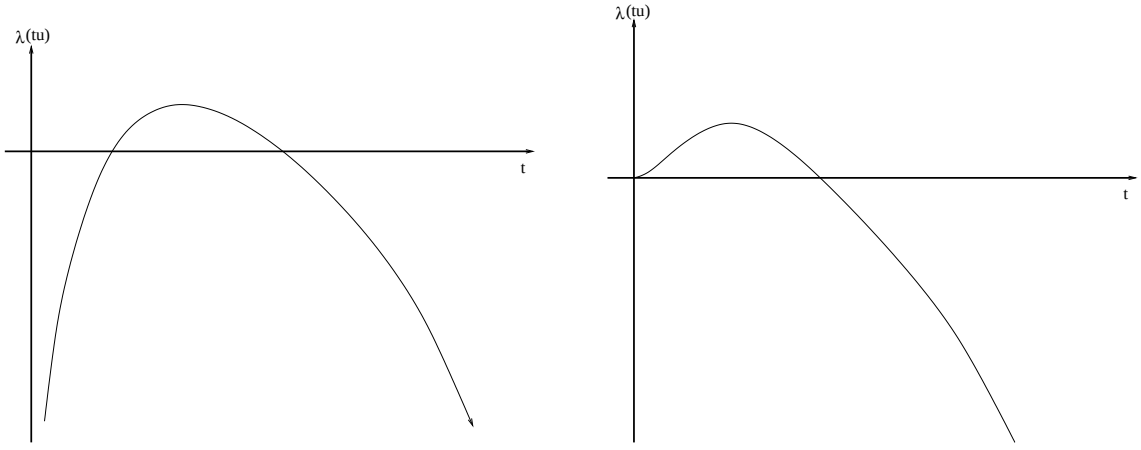

Fig. 2.1. The graph of $\lambda(tu)$ for a fixed $u \neq 0$ when $C(\lambda) = C$ (left), $C(\lambda) = C\lambda$ (right).

2.2.1 A revisit of local minimax method(LMM)

By (2.3), LMM can be applied to find critical points u of λ in the order of λ-values or their Morse indexes. Also Morse theory can be applied to discuss possible bifurcation phenomenon, which exhibits a great advantage of our approach over others.

We now briefly introduce LMM, some of its mathematical background and related results from [11,12,37,33,25,26,39]. Also some improvement needed to make the method applicable to ESP. LMM is a constrained 2-level optimization method for finding multiple critical points u of a mountain-pass type functional J in the order of J-values and their Morse indexes.

A solution characterization and Morse index

Let H be a Hilbert space and $J \in C^1(H, \mathbb{R})$. For a given closed subspace $L \subset H$, denote $H = L \oplus L^\perp$ and $S_{L^\perp} = \{v \in L^\perp : \|v\| = 1\}$. For each $v \in S_{L^\perp}$, denote $[L, v] = \text{span}\{L, v\}$.

Definition 2.2.1 *The* peak mapping $P : S_{L^\perp} \to 2^H$ *is defined by*

$$P(v) = \textit{the set of all local maxima of } J \textit{ on } [L, v], \forall v \in S_{L^\perp}.$$

A peak selection *is a single-valued mapping* $p : S_{L^\perp} \to H$ *s.t.* $p(v) \in P(v), \forall v \in S_{L^\perp}$. *If* p *is locally defined, then* p *is called a* local peak selection.

J *is said to satisfy the Palais-Smale (PS) condition in* H*, if any sequence* $\{u_n\} \subset H$ *s.t.* $\{J(u_n)\}$ *is bounded and* $J'(u_n) \to 0$ *has a convergent subsequence.*

The following theorems provide a mathematical justification for LMM and also gives an estimate for the Morse index of a solution found by LMM.

Theorem 2.2.2 *[12] If* p *is a local peak selection of* J *near* $v_0 \in S_{L^\perp}$ *s.t.* p *is locally Lipschitz continuous at* v_0 *with* $p(v_0) \notin L$ *and* $v_0 = \arg$ *local-*$\min_{v \in S_{L^\perp}} J(p(v))$ *then* $u_0 = p(v_0)$ *is a saddle point of* J*. If* p *is also differentiable at* v_0 *and we denote* $H^0 = \ker(J''(u_0))$*, then*

$$\dim(L) + 1 = MI(u_0) + \dim(H^0 \cap [L, v_0]).$$

Theorem 2.2.3 *[12] Let J be $\mathcal{C}^1$ and satisfy PS condition. If p is a peak selection of J w.r.t. L, s.t. (a) p is locally Lipschitz continuous, (b) $\inf_{x\in S_{L^\perp}} d(p(v), L) > 0$ and (c) $\inf_{v\in S_{L^\perp}} J(p(v)) > -\infty$, then there is $v_0 \in S_{L^\perp}$ s.t. $J'(p(v_0)) = 0$ and $p(v_0) = \arg\min_{v\in S_{L^\perp}} J(p(v))$.*

Let $\mathcal{M} = \{p(v) : v \in S_{L^\perp}\}$. Theorem 2.2.2 states that the process local-$\min_{u\in\mathcal{M}} J(u)$ yields a critical point u^*, which is unstable in H but stable on $\mathcal{M}$ and can be numerically approximated by, e.g., a steepest descent method. Then it leads to LMM. For $L = \{0\}$, $\mathcal{M}$ is called the *Nehari manifold* in the literature, i.e.,

$$\mathcal{N} = \{u \in H : u \neq 0, \langle J'(u), u\rangle = 0\} = \mathcal{M} = \{p(v) : v \in H, \|v\| = 1\}. \tag{2.12}$$

Verification of weaker $\mathrm{PS}_{\mathcal{N}}$ condition

PS condition is a crucial condition in proving the existence of (infinitely) multiple eigenfunctions and also the convergence of LMM. We note that $\lambda(u)$ may have a singular point. On the other hand, various PS conditions are proposed to prove the existence, but failed to handle such singularity and also not for computational purpose. According to LMM, all computations are carried only on the Nehari manifold $\mathcal{N}$, see (2.12), where it enjoys a nice property that $\langle\lambda'(u), u\rangle = 0$ for all $u \in \mathcal{N}$ and $\mathrm{dis}(\mathcal{N}, 0) > t_0 > 0$ for some $t_0 > 0$. So we can restrict our analysis only on $\mathcal{N}$ and utilize this property to simplify analysis. Such observation motivates us to introduce a new definition.

Definition 2.2.2 *A $\mathcal{C}^1$-functional J is said to satisfy $PS_{\mathcal{N}}$ condition, if any sequence $\{u_k\} \subset \mathcal{N} = \{u \in H : u \neq 0, \langle J'(u), u\rangle = 0\}$ s.t. $\{J(u_k)\}$ is bounded and $J'(u_k) \to 0$ has a convergent subsequence.*

It is clear that PS condition implies $\mathrm{PS}_{\mathcal{N}}$ condition.

Theorem 2.2.4 *$\lambda(u)$ defined in* **(1)** *or* **(2)** *satisfies $PS_{\mathcal{N}}$ condition.*

Proof Let $\{u_k\} \subset \mathcal{N}$ s.t. $\{\lambda(u_k)\}$ is bounded and $\lambda'(u_k) \to 0$. Since $C(\lambda) = C$ or $C\lambda$, $\{C(\lambda(u_k))\}$ and $\{C'(\lambda(u_k))\}$ are bounded. Note

$$H(u) = \frac{1}{2}\|\nabla u\|_{L^2}^2 - \frac{1}{p+1}\|u\|_{L^{p+1}}^{p+1}, \quad I(u) = \frac{1}{2}\|u\|_{L^2}^2.$$

We have

$$\langle I'(u_k), u_k\rangle = 2I(u_k), \quad \langle H'(u_k), u_k\rangle - 2H(u_k) = (\frac{2}{p+1} - 1)\|u_k\|_{L^{p+1}}^{p+1}.$$

Then $u_k \in \mathcal{N}$ implies

$$0 = \langle \lambda'(u_k), u_k\rangle = [I(u_k) + C'(\lambda(u_k))]^{-1}[\langle H'(u_k), u_k\rangle - \lambda(u_k)\langle I'(u_k), u_k\rangle]$$

or

$$\begin{aligned} 0 &= \langle H'(u_k), u_k\rangle - \lambda(u_k)\langle I'(u_k), u_k\rangle \\ &= \langle H'(u_k), u_k\rangle - 2H(u_k) + 2H(u_k) - 2\lambda(u_k)I(u_k) \\ &= \langle H'(u_k), u_k\rangle - 2H(u_k) + 2C(\lambda(u_k)). \end{aligned}$$

When $\{C(\lambda(u_k))\}$ is bounded, so is $\{\langle H'(u_k), u_k\rangle - 2H(u_k)\}$ and then $\{\|u_k\|_{L^{p+1}}^{p+1}\}$. By the Holder inequality $\{I(u_k)\}$ is bounded. Consequently $\{I(u_k) + C'(\lambda(u_k))\}$ is bounded, which implies that

$$\lambda'(u_k) \to 0 \Rightarrow H'(u_k) - \lambda(u_k)I'(u_k) \to 0.$$

From $H(u_k) - \lambda(u_k)I(u_k) = C(\lambda(u_k))$, we see that $\{\|\nabla u\|_{L^2}^2\}$ is bounded or $\{u_k\}$ is bounded in $H = H_0^1$. Next we follow the approach in the proof of Lemma 1.20 in

[30]. There is a subsequence, denote by $\{u_k\}$ again, and $u \in H$ s.t. $u_k \rightharpoonup u$ (means weakly) in H. By the Rellich theorem, $u_k \to u$ in L^2 and L^{p+1}. Then

$$\begin{aligned} \|u_k - u\|_H^2 &= \int_\Omega |\nabla u_k(x) - \nabla u(x)|^2 dx \\ &= \langle H'(u_k) - \lambda(u_k)I'(u_k) - H'(u) + \lambda(u)I'(u), u_k - u\rangle \\ &\quad + \langle \lambda(u_k)I'(u_k) - \lambda(u)I'(u), u_k - u\rangle + \langle u_k^p - u^p, u_k - u\rangle \to 0, \end{aligned}$$

where

$$\langle H'(u_k) - \lambda(u_k)I'(u_k) - H'(u) + \lambda(u)I'(u), u_k - u\rangle \to 0,$$

because $H'(u_k) - \lambda(u_k)I'(u_k) - H'(u) + \lambda(u)I'(u) \in H$, $H'(u_k) - \lambda(u_k)I'(u_k) \to 0$ and $u_k \rightharpoonup u$;

$$\begin{aligned} |\langle \lambda(u_k)I'(u_k) - \lambda(u)I'(u), u_k - u\rangle| &= \int_\Omega [\lambda(u_k)u_k(x) - \lambda(u)u(x)][u_k(x) - u(x)]dx \\ &\le \|\lambda(u_k)u_k - \lambda(u)u\|_{L^2}\|u_k - u\|_{L^2} \to 0, \end{aligned}$$

by the Cauchy-Schwarz inequality, the boundedness of $\lambda(u_k)$ and $u_k \to u$ in L^2; and finally

$$|\langle u_k^p - u^p, u_k - u\rangle| \le \|u_k - u\|_{L^{p+1}}^{p+1} \to 0 \quad \text{by} \quad u_k \to u \in L^{p+1}.$$

■

So Theorems 2.2.3 still hold when PS condition is replaced by $\mathrm{PS}_{\mathcal{N}}$ condition.

The numerical algorithm and its Convergence

Let $w_1, ..., w_{n-1}$ be n-1 previously found critical points, $L = [w_1, ..., w_{n-1}]$. Given $\varepsilon > 0, \ell > 0$ and $v^0 \in S_{L^\perp}$ be an ascent-descent direction at w_{n-1}.

Step 1: Let $t_0^0 = 1, v_L^0 = 0$ and set $k = 0$;

Step 2: Using the initial guess $w = t_0^k v^k + v_L^k$, solve for

$$w^k \equiv p(v^k) = \arg \max_{u \in [L, v^k]} J(u) \text{ and denote } t_0^k v^k + v_L^k = w^k \equiv p(v^k);$$

Step 3: Compute the steepest descent vector $d^k := -J'(w^k)$;

Step 4: If $\|d^k\| \leq \varepsilon$ then output $w_n = w^k$, stop; else goto Step 5;

Step 5: Set $v^k(s) := \dfrac{v^k + sd^k}{\|v^k + sd^k\|} \in S_{L^\perp}$ and find

$$s^k := \max_{m\in\mathbb{N}} \left\{ \frac{\ell}{2^m} : 2^m > \|d^k\|, J(p(v^k(\frac{\ell}{2^m}))) - J(w^k) \leq -\frac{t_0^k \ell}{2^{m+1}}\|d^k\|^2 \right\}.$$

Initial guess $u = t_0^k v^k(\frac{\ell}{2^m}) + v_L^k$ is used to find (track a peak selection) $p(v^k(\frac{\ell}{2^m}))$ where t_0^k and v_L^k are found in **Step 2**;

Step 6: Set $v^{k+1} = v^k(s^k), w^{k+1} = p(v^{k+1}), k = k+1$, then goto **Step 3**.

Remark 2.2.2 *$\ell > 0$ controls the maximum stepsize of each search. The condition $v^0 \in S_{L^\perp}$ does not have to be exact and actually can be relaxed. LMM first starts with $n = 0, L = \{0\}$ to find a solution w_1. Then LMM starts with $n = 1, L = span\{w_1\}$ to find another solution w_2. LMM continues in this way with L gradually expanded by previously found solutions.*

Convergence of the algorithm is established by the following theorem. The main frame of the theorem remains the same as in ([39]), despite original PS condition is replaced by $\mathrm{PS}_{\mathcal{N}}$ condition here.

Theorem 2.2.5 *If J is $\mathcal{C}^1$ and satisfies $PS_{\mathcal{N}}$ condition, (a) p is locally Lipschitz continuous, (b) $d(L, p(v^k)) > \alpha > 0$ and (c) $\inf\limits_{v\in S_{L^\perp}} J(p(v)) > -\infty$, then $v^k \to v^* \in S_{L^\perp}$ with $\nabla J(p(v^*)) = 0$.*

2.2.2 The focusing Schrödinger ESP with zero Dirichlet B.C.

For our LMM to success, it is important to show that all approximation solutions in LMM will be kept a positive distance away from $u = 0$.

Theorem 2.2.6 *Let λ be given in* **(1)** *or* **(2)**. *There is $t_0 > 0$ s.t. for all $u \in H = H_0^1(\Omega)$ with $\|u\|_H = 1$, there is a unique $t_u > t_0$ satisfying $\frac{d\lambda(tu)}{dt}|_{t=t_u} = 0$. Furthermore in either case the peak selection p is unique and differentiable when $L = \{0\}$ and satisfies $\|p(u)\| > t_0$.*

Proof Note $\|u\|_H = \|\nabla u\|_{L^2} = 1$. By the Sobolev inequality, let $C_s > 0$ be the constant s.t. $\|u\|_{L^s}^s < C_s \, \forall u \in H, \|u\|_H = 1$. **(1)** For $C(\lambda) = C > 0$, we have

$$\lambda(tu) = \frac{H(tu) - C}{I(tu)} = \frac{1}{\|u\|_{L^2}^2}\Big[1 - \frac{2}{p+1}t^{p-1}\|u\|_{L^{p+1}}^{p+1} - 2Ct^{-2}\Big]$$

and

$$\begin{aligned}\frac{d}{dt}\lambda(tu) &= \frac{1}{\|u\|_{L^2}^2}\Big[-\frac{2(p-1)}{p+1}t^{p-2}\|u\|_{L^{p+1}}^{p+1} + 4Ct^{-3}\Big] \\ &> \frac{1}{\|u\|_{L^2}^2}\Big[(-\frac{2(p-1)}{p+1}C_{p+1}t^{p+1} + 4C)t^{-3}\Big].\end{aligned}$$

Thus there is $t_0 > 0$ s.t. when $0 < t < t_0$, we have

$$\frac{d}{dt}\lambda(tu) > 0 \quad \text{or} \quad t_u > t_0 \, \forall u \in H, \|u\|_H = 1.$$

(2) For $C(\lambda) = C\lambda$, we have

$$\lambda(tu) = \Big[\frac{t^2}{2}\|u\|_{L^2}^2 + C\Big]^{-1}\Big(\frac{t^2}{2} - \frac{t^{p+1}}{p+1}\|u\|_{L^{p+1}}^{p+1}\Big)$$

$$\begin{aligned}\frac{d}{dt}\lambda(tu) &= \Big[\frac{t^2}{2}\|u\|_{L^2}^2 + C\Big]^{-2}\Big[t^{p+2}(\frac{1}{p+1} - \frac{1}{2})\|u\|_{L^{p+1}}^{p+1}\|u\|_{L^2}^2 + C(t - t^p\|u\|_{L^{p+1}}^{p+1})\Big] \\ &> [\frac{t^2}{2}\|u\|_{L^2}^2 + C]^{-2}\Big[t^{p+2}(\frac{1}{p+1} - \frac{1}{2})C_{p+1}C_2 - t^pCC_{p+1} + Ct\Big].\end{aligned}$$

Thus there is $t_0 > 0$ s.t. when $0 < t < t_0$, it holds

$$\frac{d}{dt}\lambda(tu) > 0 \quad \text{or} \quad t_u > t_0 \; \forall u \in H, \|u\|_H = 1.$$

On the other hand, for either case **(1)** or case **(2)**, we have

$$\frac{d}{dt}\lambda(tu) = \langle \lambda'(tu), u\rangle = [\langle H'(tu), u\rangle - \lambda(tu)\langle I'(tu), u\rangle][I(tu) + C'(\lambda(tu))]^{-1}.$$

At $t = t_u > 0$, we have $\frac{d\lambda(tu)}{dt}|_{t=t_u} = \langle \lambda'(t_u u), u\rangle = 0$ or $\langle H'(t_u u), u\rangle = \lambda(t_u u)\langle I'(t_u u), u\rangle$ and

$$\begin{aligned} & \frac{d^2}{dt^2}\lambda(tu)|_{t=t_u} = \langle \lambda''(t_u u)u, u\rangle \\ = \; & [\langle H''(t_u u), u\rangle - \lambda(t_u u)\langle I''(t_u u), u\rangle][I(t_u u) + C'(\lambda(t_u u))]^{-1}. \end{aligned}$$

Note that

$$\begin{aligned} t_u\langle H''(t_u u)u, u\rangle &= t_u \int_\Omega [|\nabla u(x)|^2 - p t_u^{p-1}|u(x)|^{p+1}]dx \quad \forall p > 1 \\ &< \int_\Omega [t_u|\nabla u(x)|^2 - t_u^p|u(x)|^{p+1}]dx = \langle H'(t_u u), u\rangle \\ &= \lambda(t_u)\langle I'(t_u u), u\rangle \\ &= \lambda(t_u u)\int_\Omega t_u u^2(x)dx = t_u\lambda(t_u u)\langle I''(t_u u)u, u\rangle. \end{aligned}$$

Since $I(t_u u) + C'(\lambda(t_u u)) > 0$, we conclude that

$$\frac{d^2}{dt^2}\lambda(tu)|_{t=t_u} < 0, \tag{2.13}$$

which implies that $t_u > 0$ is unique and also in either case **(1)** or case **(2)**, by the implicit function theorem, the peak selection p when $L = \{0\}$ is unique and differentiable, or the Nehari manifold $\mathcal{N}$ is differentiable. Since when $L = \{0\}$,

$p(u) = t_u u$, we have $\|p(u)\|_H = t_u > t_0 > 0 \; \forall u \in H$ with $\|u\|_H = 1$ or $\text{dist}(0, \mathcal{N}) > t_0$. ■

The steepest descent direction $d = \nabla\lambda$ at u in Step 3 of LMM is solved in $H_0^1(\Omega)$ from

$$\begin{aligned} -\Delta d(x) &= [I(u)]^{-1}[H'(u) - \lambda(u)I'(u)] \\ &= [\frac{1}{2}\int_\Omega u^2(x)dx]^{-1}[-\Delta u(x) - |u(x)|^{p-1}u(x) - \lambda(u)u(x)]. \end{aligned}$$

This is where a numerical linear elliptic solver can be applied, e.g., a finite difference method (FDM), a finite element method (FEM) or a finite boundary element method (FBEM). We use a Matlab subroutine "assempde", a finite element method in our numerical computation.

Numerical Results

Let $\Omega = (-0.5, 0.5)^2, p = 3, \varepsilon = 10^{-5}$, $H(u) = \int_\Omega [\frac{1}{2}\nabla u(x)|^2 - \frac{1}{4}u^4(x)^4]dx$, $I(u) = \int_\Omega \frac{1}{2}u^2(x)dx$ and $J(u) = H(u) - \lambda I(u) = C(\lambda)$. We carry out numerical computation for **Case (1)**: $C(\lambda) = C = 10, 20$ and **Case (2)**: $C(\lambda) = C\lambda$ with $C = 1, 2$. An initial guess u_0 is solved from $-\Delta u + u = f(x)$ on Ω and $u(x) = 0$ on $\partial\Omega$, where $f(x) = -1, 1$ or 0 if one wants u_0 to be concave up, concave down or flat at $x \in \Omega$. The support is selected as $L(u_1) = \{0\}$ and $L(u_i) = [u_1, ..., u_{i-1}]$. All numerical computations went through smoothly. For easy comparison, we put all λ and $\|u\|$-values in Table 2.1. Due to the symmetry of the problem, for each eigenfunction we present only a representative of its equivalent class in the figures, Fig. 2.2;2.3;2.4;2.5.

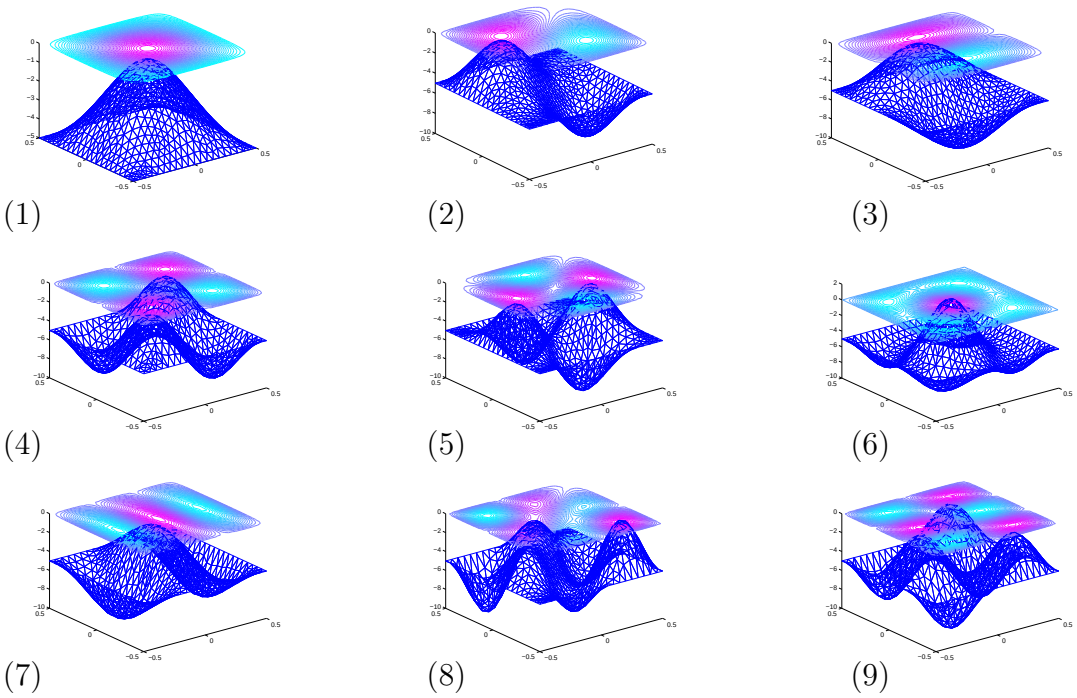

Fig. 2.2. Case 1. $C = 10$. Profiles and contours of eigenfunctions $u_1, ..., u_9$.

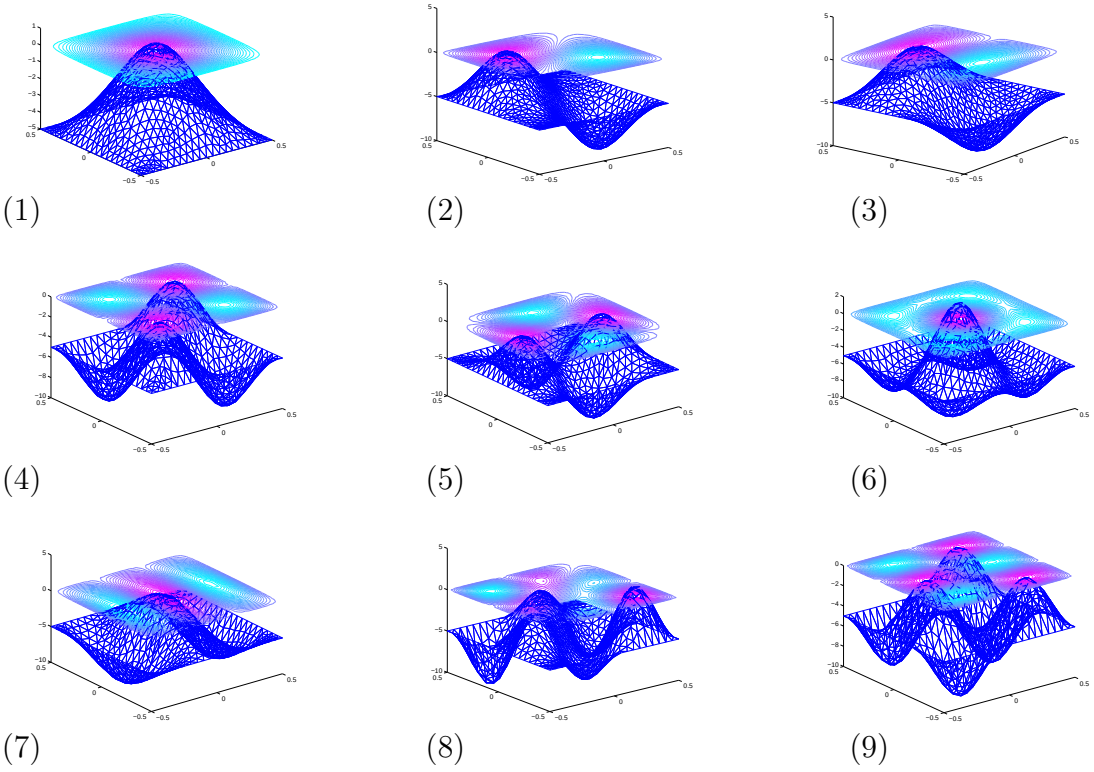

(1) (2) (3)

(4) (5) (6)

(7) (8) (9)

Fig. 2.3. Case 1. $C = 20$. Profiles and contours of eigenfunctions $u_1, ..., u_9$.

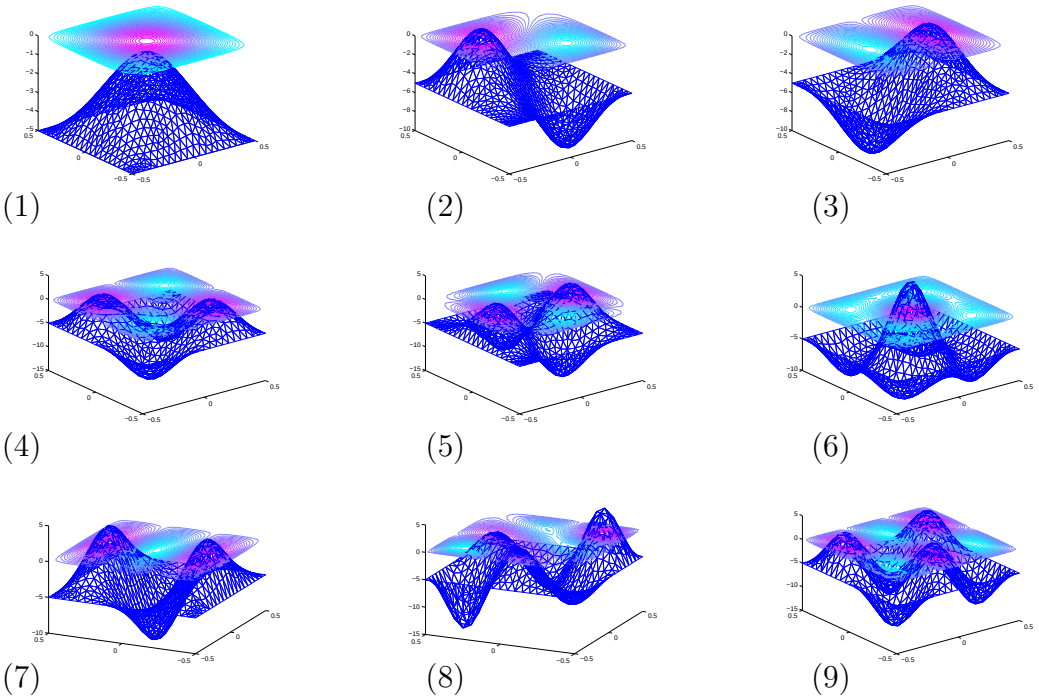

Fig. 2.4. Case 2. $C = 1$. Profiles and contours of eigenfunctions $u_1, ..., u_9$.

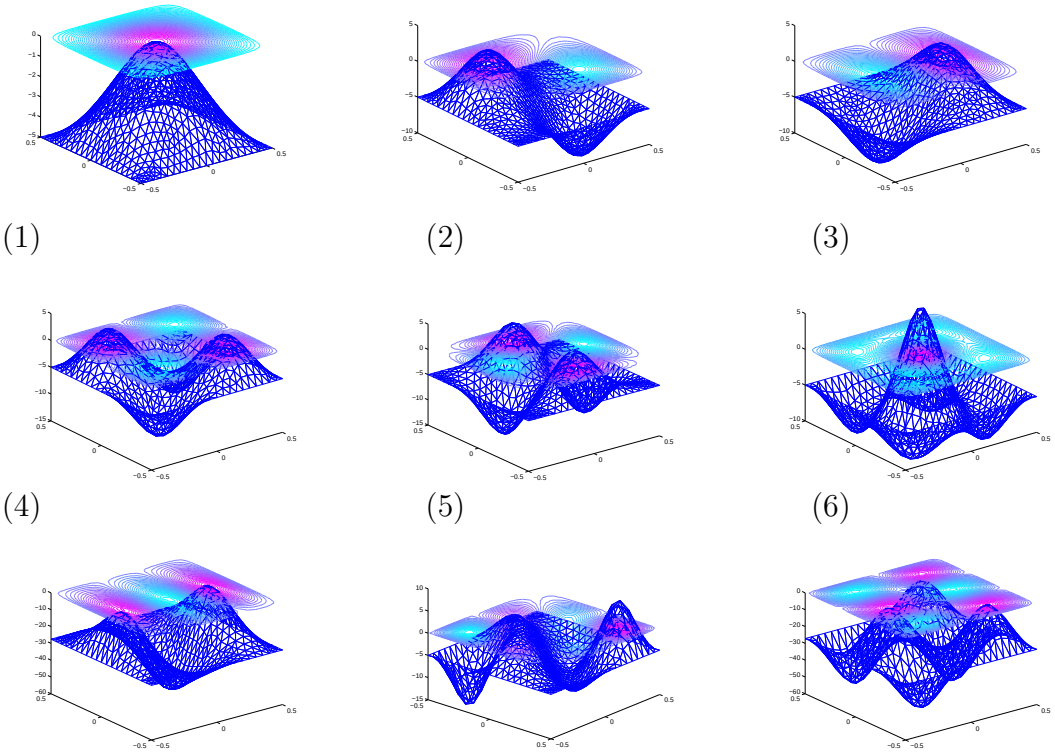

(1) (2) (3)

(4) (5) (6)

(7) (8) (9)

Fig. 2.5. Case 2. $C = 2$. Profiles and contours of eigenfunctions $u_1, ..., u_9$.

Table 2.1
Numerical result of focusing Schrödinger ESP with zero Dirichlet B.C.

	Case (1): $C(\lambda) = C$				Case (2): $C(\lambda) = C\lambda$			
	$C = 10$		$C = 20$		$C = 1$		$C = 2$	
k	λ_k	$\|u_k\|$	λ_k	$\|u_k\|$	λ_k	$\|u_k\|$	λ_k	$\|u_k\|$
1	9.9594	9.1264	5.6939	10.7764	9.9731	9.1205	7.5888	10.0862
2	38.9635	13.8164	34.5421	16.3379	30.8403	18.1271	25.3741	20.4135
3	39.7149	14.3249	35.5935	16.9138	31.8415	18.8809	26.4798	21.2664
4	69.4852	18.2481	65.4870	21.6431	56.1634	27.8533	48.7244	31.8310
5	88.4921	19.5903	84.1640	23.2262	70.9239	31.5970	61.7317	36.0982
6	88.5404	19.6912	84.2720	23.4078	71.3244	32.1891	62.4561	37.0861
7	89.1777	20.1890	85.0800	23.8356	72.0392	32.0738	62.7393	36.3035
8	118.2005	22.3240	113.8775	26.4678	95.9733	38.6666	84.7947	44.1722
9	118.9864	23.2559	115.0084	27.6010	98.2867	40.7662	87.8495	46.9151

2.2.3 The focusing Schrödinger ESP with zero Neumann B.C.

Since ESP (1.9) is also related to systems in chemotaxis or other chemical or biological diffusion process [6, 10, 13, 20] where a Neumann B.C. is prescribed, in this section, we solve

$$-\Delta u(x) - \beta|u(x)|^{p-1}u(x) = \lambda u(x), \quad x \in \Omega, \quad u \in H = H^1(\Omega), \tag{2.14}$$

satisfying a zero Neumann B.C. where $\beta > 0$ is a parameter. It is clear that if (u, λ) is an eigen solution, then so is $(-u, \lambda)$. Due to the application background, we are interested mainly in the positive eigenfunctions, although mathematically there are sign-changing eigenfunctions, which may interfere our efforts to compute positive ones. The variational functional becomes

$$J(u) = H(u) - \lambda(u)I(u) = C \tag{2.15}$$

where $H(u) = \frac{1}{2}\|\nabla u\|_{L^2}^2 - \frac{\beta}{p+1}\|u\|_{L^{p+1}}^{p+1}$, and $I(u) = \frac{1}{2}\|u\|_{L^2}^2$. Integrating (2.14) for a one-sign eigenfunction u and applying the zero Neumann B.C. lead to

$$-\beta \int_\Omega |u(x)|^{p-1}u(x)dx = \lambda \int_\Omega u(x)dx,$$

which indicates $\lambda < 0$ for all one-sign eigenfunctions. But a sign-changing eigenfunction u may still have a positive eigenvalue. Since we need $C(\lambda) > 0$ and $C'(\lambda) \geq 0$ in our setting, we consider only the case $C(\lambda) = C > 0$. Multiplying u to (2.14) and integrating it, then comparing to (2.15), we obtain

$$[\frac{1}{2} - \frac{1}{p}]\beta\|u\|_{L^{p+1}}^{p+1} = C \tag{2.16}$$

for all eigenfunctions u, i.e., $\|u\|_{L^{p+1}} = C_p > 0$ for some constant $C_p > 0$. Then $\|u\|_{L^2} < C_h$ for some constant $C_h > 0$ by the Holder inequality. Consequently from (2.14), we have

$$\|\nabla u\|_{L^2}^2 - \lambda\|u\|_{L^2}^2 = \frac{2p}{p-2}C$$

which implies, for all eigenfunctions u with $\lambda < 0$, $\|\nabla u\|_{L^2}$ is bounded. We have proved

Proposition 2.2.1 *For ESP (2.14), in addition to the results in Theorem 2.2.1, it holds that $\{\|u_k\|_H\}$ is bounded for all positive eigenfunctions u_k and sign-changing eigenfunctions u_k with $\lambda < 0$.*

Note that the proof of the first part of Theorem 2.2.6 utilizes the Sobolev inequality which is valid for functions in H with a zero Dirichlet B.C. but not valid for functions in H with a zero Neumann B.C. So we have to use other properties instead. Under the equality in (2.16), without loss of generality, we may assume that for each fixed $C > 0$, let $M_C > 0$ be a very large number and consider only the closed set

$$U = \{u \in H = H^1(\Omega) : \|u\|_{L^{p+1}}^{p+1} \leq M_C\}.$$

Theorem 2.2.7 *Let*

$$\lambda(tu) = \frac{H(tu) - C}{I(tu)} = \frac{\|\nabla u\|_{L^2}^2 - \frac{2t^{p-1}}{p+1}\|u\|_{L^{p+1}}^{p+1} - 2Ct^{-2}}{\|u\|_{L^2}^2}$$

for each $u \in U$ with $\|u\|_H = 1$ and $t > 0$. There is $t_0 > 0$ s.t. for all $u \in U$ with $\|u\|_H = 1$, there exists a unique $t_u > t_0$ satisfying $\frac{d\lambda(tu)}{dt}|_{t=t_u} = 0$. Furthermore in either case the peak selection p is unique and differentiable when $L = \{0\}$ and satisfies $\|p(u)\| > t_0$.

Proof We have

$$\begin{aligned} \frac{d}{dt}\lambda(tu) &= \frac{1}{\|u\|_{L^2}^2}\Big[-\frac{2(p-1)}{p+1}t^{p-2}\|u\|_{L^{p+1}}^{p+1} + 4Ct^{-3}\Big] \\ &\geq \frac{1}{\|u\|_{L^2}^2}\Big[(-\frac{2(p-1)}{p+1}t^{p+1}M_c + 4C)t^{-3}\Big], \end{aligned}$$

since $u \in U$ or $\|u\|_{L^{p+1}}^{p+1} \leq M_C$. Thus there is $t_0 > 0$ s.t. when $0 < t < t_0$, we have

$$\frac{d}{dt}\lambda(tu) > 0 \quad \text{or} \quad t_u > t_0 \; \forall u \in U, \|u\|_H = 1.$$

Note that the proof of the inequality (2.13) in Theorem 2.2.6 does not involve the Sobolev inequality, so it is still valid in the current situation and the rest of the theorem follows. ■

It is known that solutions to Neumann boundary value problems exhibit drastically different behavior to their Dirichlet counterparts. The numerical computation in this subsection becomes even more complicated due to the existence of a positive constant eigenfunction u_C. Many of our numerical experiments suggest that when the value of C varies, $\mathrm{MI}(u_C)$ changes and results in possible bifurcation from u_C to many positive eigenfunctions or multiple branches of eigenfunctions. Such a situation causes tremendous difficulty for us to set up the support L in LMM. In order to have successful numerical results, we must do more analysis about this situation and

have a better understanding. The following analysis displays a significant advantage of our approach over others in the literature. Let $0 = \mu_1 < \mu_2 \leq \mu_3 \leq \cdots$ be the eigenvalues of the linear ESP

$$-\triangle u(x) = \mu u(x) \quad x \in \Omega \quad \text{and} \quad \frac{\partial u(x)}{\partial n} = 0 \quad x \in \partial\Omega. \tag{2.17}$$

Theorem 2.2.8 *Let C be $\mathcal{C}^2$ with $C'(\lambda) > 0$ and $\lambda(u)$ be the function implicitly defined by the equation*

$$H(u) - \lambda(u)I(u) = C(\lambda(u))$$

where $H(u)$ and $I(u)$ are given in (2.15) and u_C be a positive constant solution to

$$\lambda'(u) \equiv \frac{H'(u) - \lambda(u)I'(u)}{I(u) + C'(\lambda(u))} = 0.$$

For $k = 1, 2, 3, ...,$

(a) if $\mu_k < (p-1)\beta u_C^{p-1} < \mu_{k+1}$, then u_C is nondegenerate with $MI(u_C) = k$;

(b) if $\mu_k < (p-1)\beta u_C^{p-1} = \mu_{k+1} = \cdots = \mu_{k+1+r_k} < \mu_{k+2+r_k}$, then u_C is degenerate with $MI(u_\varepsilon^1) = k$ and nullity$(u_C) = r_k \geq 1$ and bifurcates to new positive solution(s).

Furthermore if $C(\lambda) = C > 0$, then

$$u_C = \Big[\frac{2C(p+1)}{|\Omega|\beta(p-1)}\Big]^{\frac{1}{p+1}}, \quad \lambda(u_C) = -\beta\Big[\frac{2C(p+1)}{|\Omega|\beta(p-1)}\Big]^{\frac{p-1}{p+1}} \tag{2.18}$$

and u_C is monotonically increasing in C. So C is a bifurcation parameter and there is a (respectively no) bifurcation taking place for u_C under the condition (b) (respectively (a)).

Proof We have an expression for the linear operator

$$\begin{aligned}\lambda''(u) &= \frac{1}{(I(u)+C'(\lambda(u))^2}[(H''(u)-\lambda'(u)I'(u)-\lambda(u)I''(u))(I(u)+C'(\lambda(u)) \\ &\quad -(I'(u)+C''(\lambda(u))\lambda'(u))(H'(u)-\lambda(u)I'(u))].\end{aligned}$$

At each u s.t. $\lambda'(u)=0$ or $H'(u)-\lambda(u)I'(u)=0$, we have

$$\lambda''(u)=\frac{H''(u)-\lambda(u)I''(u)}{I(u)+C'(\lambda(u))}.$$

Taking $H(u)=\int_\Omega(\frac{1}{2}|\nabla u(x)|^2-\frac{\beta}{p+1}|u(x)|^{p+1})dx, I(u)=\int_\Omega \frac{1}{2}u^2(x)dx$ into account, we have

$$H'(u)=\Delta u-\beta|u|^{p-1}u,\ I'(u)=u,\ H''(u)w=-\Delta w-p\beta|u|^{p-1}w,\ I''(u)w=w$$

and then

(2.19)

$$\lambda'(u_C)=0 \Leftrightarrow H'(u_c)-\lambda(u_C)I'(u_C)=0 \Leftrightarrow -\beta u_C^p-\lambda(u_C)u_C=0 \Leftrightarrow \lambda(u_C)=-\beta u_C^{p-1}.$$

Note $u_C>0$ can be solved from

(2.20)

$$H(u_C)-\lambda(u_C)I(u_C)=C(\lambda(u_C)) \text{ or } -\frac{\beta}{p+1}u_C^{p+1}|\Omega|+u_C^{p-1}\frac{\beta}{2}u_C^2|\Omega|=C(-\beta u_C^{p-1}).$$

Let η be an eigenvalue of the linear operator $\lambda''(u_C)$ and w be an associated eigenfunction, i.e.,

$$\lambda''(u_C)w=\frac{-\Delta w-p\beta u_C^{p-1}w+\beta u_C^{p-1}w}{\frac{1}{2}u_C^2|\Omega|+C'(-u_C^{p-1})}=\eta w.$$

It leads to

$$-\Delta w=[(p-1)\beta u_C^{p-1}+\eta(\frac{1}{2}u_C^2|\Omega|+C'(-u_C^{p-1}))]w=\mu w,$$

where μ is an eigenvalue of $-\Delta$ and w is its associated eigenfunction. So $\lambda''(u_C)$ and $-\Delta$ share exactly the same eigenfunctions. We must have

$$\eta = \frac{\mu - (p-1)\beta u_C^{p-1}}{\frac{1}{2}u_C^2|\Omega| + C'(-u_C^{p-1})},$$

which indicates that η and μ have the same multiplicity. Let $\eta_1 < \eta_2 \leq \eta_3 \cdots$ be all the eigenvalues of $\lambda''(u_C)$. We obtain that for $k = 1, 2, \cdots$, (a) if

$$\mu_k < (p-1)\beta u_C^{p-1} < \mu_{k+1}, \tag{2.21}$$

then $\eta_i < 0, i = 1, 2, ..., k$ and $\eta_j > 0, j = k+1, k+2, ...,$ thus u_C is nondegenerate with $\mathrm{MI}(u_c) = k$ and (b) if

$$\mu_k < (p-1)\beta u_C^{p-1} = \mu_{k+1} = \cdots = \mu_{k+r_k} < \mu_{k+1+r_k}, \tag{2.22}$$

then $\eta_i < 0, i = 1, 2, ..., k, \eta_i = 0, i = k+1, ..., k+r_k, \eta_i > 0, i = k+1+r_k, k+2+r_k, ...,$ thus u_c is degenerate with $\mathrm{MI}(u_C) = k$, $\mathrm{nullity}(u_C) = r_k \geq 1$ and u_C bifurcates to new solution(s) [7]. Note that by the maximum principle, an one-sign solution either whose value and derivative are equal to zero at an interior point of Ω or whose value and normal derivative are equal to zero at a boundary point of Ω must be identically equal to zero. Since a sign-changing solution has nodal line(s) (where values are equal to zero) inside Ω, when a sequence of sign-changing solutions approach to an one-sign solution u^*, there are two possibilities: (1) some nodal lines stay inside Ω thus u^* attains its zero value and zero derivative at an interior point of Ω or (2) some nodal lines approach to the boundary $\partial\Omega$ thus u^* attains its zero value and zero normal derivative (as a solution) at a boundary point of Ω. In either case, u^* has to be identically equal to zero. When

$$\mu_1 = 0 < (p-1)\beta u_C^{p-1} < \mu_2$$

u_C is nondegenerate, so no bifurcation takes place. On the other hand, since $u_C > 0 = \mu_1$ and at each bifurcation point $(p-1)\beta u_C^{p-1} = \mu_{k+1} \geq \mu_2 > 0$, $u_C > 0$ must satisfy

$$u_C \geq \Big[\frac{\mu_2}{(p-1)\beta}\Big]^{\frac{1}{p-1}} > 0$$

and can bifurcate only to positive non trivial solutions. See Fig 2.6.

When $C(\lambda) = C$, the equation in (2.20) becomes

$$-\frac{\beta}{p+1}u_C^{p+1}|\Omega| + u_C^{p-1}\frac{\beta}{2}u_C^2|\Omega| = C,$$

which leads to

$$u_C = \Big[\frac{2C(p+1)}{|\Omega|\beta(p-1)}\Big]^{\frac{1}{p+1}} \quad \text{and} \quad \lambda(u_C) = -\beta\Big[\frac{2C(p+1)}{|\Omega|\beta(p-1)}\Big]^{\frac{p-1}{p+1}} \tag{2.23}$$

from the last equation in (2.19). It is clear that u_C is monotonically increasing in C. When C increases so that the term $(p-1)u_C^{p-1}$ increases and crosses each μ_k, the positive constant solution u_C bifurcates to new positive solution(s). ■

Remark 2.2.3 *Using (2.18), the term in (a) and (b) of Theorem 2.2.8 becomes*

$$(p-1)\beta u_C^{p-1} = \beta^{\frac{2}{p+1}}(p-1)\Big[\frac{2C(p+1)}{|\Omega|(p-1)}\Big]^{\frac{p-1}{p+1}}.$$

Thus β can also be viewed as a bifurcation parameter, i.e., when β increases, u_C bifurcates to positive eigenfunctions. However in this paper, we fix β as a constant and only let C vary.

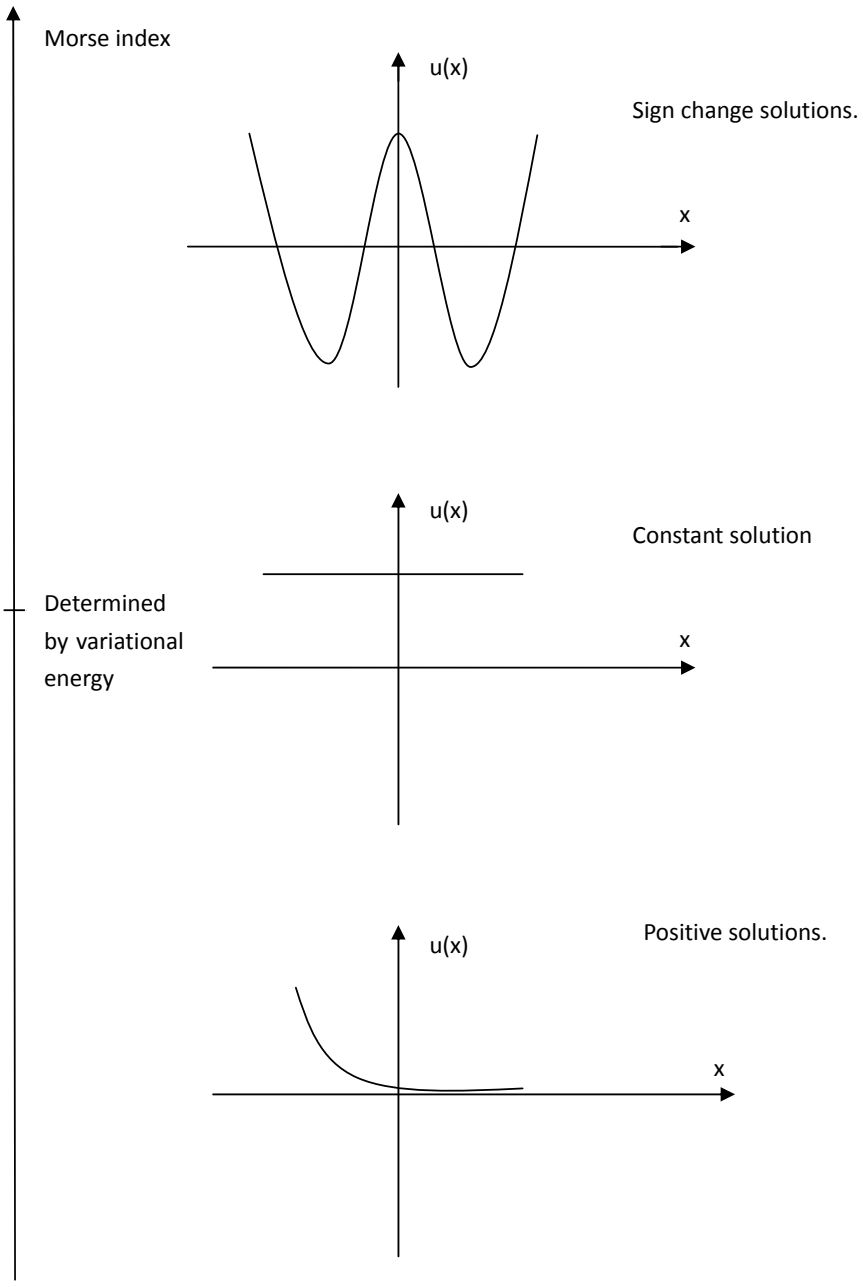

Fig. 2.6. Solutions according to their Morse index.

Numerical results

In (2.14), we choose $\Omega = (-0.5, 0.5)^2, \beta = 5, p = 3, \varepsilon = 10^{-5}$. So the eigenvalues in (2.17) are given by the formula $\mu_{(n,m)} = (n\pi)^2 + (m\pi)^2$ for $n, m = 0, 1, 2, 3, ...$, or, in a sequential order, $\mu_1 = \mu_{(0,0)} = 0$, $\mu_2 = \mu_{(0,1)} = \mu_{(1,0)} = 9.8696, \mu_3 = \mu_{(1,1)} = 19.7392$, $\mu_4 = \mu_{(0,2)} = \mu_{(2,0)} = 39.4784$, $\mu_5 = \mu_{(1,2)} = \mu_{(2,1)} = 49.3480, ..., \mu_8 = \mu_{(1,3)} = \mu_{(1,3)} = 90.8696, \mu_9 = \mu_{(2,3)} = \mu_{(3,2)} = 128.3049$. In our numerical computation we deliberately choose C-values and check the inequality

$$\mu_k < (p-1)\beta u_C^{p-1} = 10u_C^2 < \mu_{k+1}$$

for some $k = 1, 2, ...$, so that each example represents a typical case and we can apply the bifurcation result, Theorem 2.2.8 to predict the existence of certain positive eigenfunctions and to decide the support L in LMM to find them. Since all other positive eigenfunctions are bifurcated from u_C, we have $\lambda(u) < \lambda(u_C)$ for all positive eigenfunctions u. So when $\lambda(u_C) - \lambda(u)$ is very small, it indicates that there is no other positive eigenfunction in between.

The steepest descent direction $d = \nabla\lambda$ at a given u in Step 3 of LMM is solved from

$$\begin{aligned} -\Delta d(x) + d(x) &= [I(u)]^{-1}[H'(u) - \lambda(u)I'(u)] \\ &= [\frac{1}{2}\int_\Omega u^2(x)dx]^{-1}[-\Delta u(x) - |u(x)|^{p-1}u(x) - \lambda(u)u(x)] \end{aligned}$$

in $H^1(\Omega)$ satisfying a zero Neumann B.C.. In our numerical computation this linear elliptic equation is solved by calling a Matlab subroutine "assempde", a finite element method.

For the problem (2.4) with zero Dirichlet B.C., the peak(s) of an eigenfunction is (are) always located inside Ω. However for the problem (2.14), one can see that most

eigenfunctions have their peak(s) located on the boundary of Ω, but occasionally some eigenfunctions may have their peak(s) located inside Ω.

Note that the problem (2.14) possesses the symmetries on rotations by $\frac{\pi}{2}, \pi, \frac{2\pi}{2}, 2\pi$ and reflections about the axes $x = 0, y = 0, y = x, y = -x$. In the following figures, we show only one eigenfunction representing its equivalent class, e.g., when we set $L = \{u_1\}$ we may actually use an eigenfunction in the equivalent class of u_1. To compute sign-changing eigenfunctions of (2.14), we use their corresponding eigenfunctions of $-\Delta$ as initial guesses. Since there is no eigenfunction of $-\Delta$ corresponding to a nontrivial positive eigenfunction of (2.14), we first guess an initial u_0 with certain peak location by setting suitable $f(x) = -1, 1$ or 0 if one wants u_0 to be concave up, concave down or flat at $x \in \Omega$ and then solve u_0 from $-\Delta u + u = f(x)$ on Ω with a zero Neumann B.C. We indicate this process by IPL.

In Fig.2.7, we set $C = 0.25$, $L(u_1) = \{0\}, L(u_2) = \{u_1\}, L(u_3) = \{u_1\}, L(u_4) = \{u_1, u_2\}$, $L(u_5) = \{u_1, u_2, u_4\}, L(u_6) = \{u_1, u_2, u_4, u_5\}, L(u_7) = \{u_1, u_2, u_4, u_5, u_6\}$ and $u_0^1 = \sqrt{5}, u_0^2 = \frac{\pi}{2}(sin(x_1\pi)+sin(x_2\pi)), u_0^3 = \pi sin(x_1\pi), u_0^4 = \pi^2 sin(x_1\pi)sin(x_2\pi)$, $u_0^5 = 2\pi cos(2x_1\pi)$, $u_0^6 = 2\pi(cos(2x_1\pi) + cos(2x_2\pi)), u_0^7 = -4\pi cos(4x_1\pi)$. Since $u_C = 0.6687$ and $0 = \mu_1 < 10u_C^2 = 4.4715 < \mu_2 = 9.8696$, no bifurcation takes place. Thus u_C is the only positive eigenfunction and sign-changing eigenfunctions can be smoothly computed

In Fig.2.8, we set $C = 1.25$, $L(u_1) = \{0\}, L(u_2) = \{u_1\}, L(u_3) = \{0\}, L(u_4) = \{u_3\}$ and $u_0^i = \text{IPL}, \frac{\pi}{2}(sin(x_1\pi) + sin(x_2\pi)), \pi sin(x_1\pi), \pi^2 sin(x_1\pi)sin(x_2\pi)$. Since $u_C = 1$ and $9.8696 = \mu_2 < 10u_C^2 = 10 < \mu_3 = 19.7392$, u_C bifurcates to u_1 and its rotations by $\frac{\pi}{2}, \pi, \frac{3\pi}{2}$. Also $\lambda(u_C) - \lambda(u_1)$ is very small, so no other positive eigenfunction is in between.

In Fig.2.9, we set $C = 7$, $L(u_1) = L(u_2) = \{0\}, L(u_3) = \{u_1\}$ and $u_0^i = \text{IPL}$. Since $u_C = 1.5382$ and $19.7392 = \mu_3 < 10u_C^2 = 23.6605 < \mu_4 = 39.4784$, we find three nontrivial positive eigenfunctions.

In Fig.2.10, we set $C = 20$, $L(u_1) = L(u_3) = \{0\}, L(u_2) = \{u_1\}, L(u_4) = \{u_3\}$ and $u_0^i = \text{IPL}, \frac{\pi}{2}(sin(x_1\pi) + sin(x_2\pi)), 2, \pi sin(x_1\pi)$. Since $u_C = 2$ and $39.4784 = \mu_4 < 10u_C^2 = 40 < \mu_5 = 49.3480$, positive and sign-changing eigenfunctions appear mixed in the sequential order. The order becomes much more complicated.

Next we further increase the C-value. Since there are too many sign-changing eigenfunctions in between positive ones, it is too difficult to follow the whole order to find eigenfunctions. However we are still able to know the order of positive eigenfunctions by our bifurcation theorem and their symmetries. So we focus on finding positive eigenfunctions. In order to reduce the dimension of L, we use the symmetry of the problem and apply a Haar projection (HP) in LMM, see [25] for more details. Meanwhile when C is larger, the peak(s) of an eigenfunction becomes more sharp and narrow. An uniform finite element mesh may loss its accuracy. Thus local mesh refinements are used in our numerical computation when necessary. In order to see the profiles and their contours clearer, figures presented below are regenerated on a uniform coarse mesh and shifted downward.

In Fig.2.11, we set $C = 25$, $L(u_i) = \{0\}, i = 1, 2, 5, 6, L(u_3) = \{u_1\}, L(u_6) = \{u_2\}$ and all $u_0^i = \text{IPL}$. We have used HP to compute u_6. Since $u_C = 2.1147$ and $39.4784 = \mu_4 < 10u_C^2 = 44.7212 < \mu_5 = 49.3480$, more positive eigenfunctions appeared due to bifurcations from u_C.

In Fig.2.12, we set $C = 125$, $L(u_i) = \{0\}, i = 1, 2, 4, 7, 8, 9, 10$, $L(u_3) = L(u_5) = L(u_6) = \{u_1\}$ and $u_0^i = \text{IPL}$. Since $u_C = 3.1623$ and $90.8696 = \mu_8 < 10u_C^2 = 100 < \mu_9 = 128.3049$, more eigenvalues μ_k are passed. Thus even more positive eigenfunctions appeared. We have used HP in LMM with $L = \{0\}$ to compute u_2, u_6, u_7, u_8, u_{10}. However since u_1 and u_6 have exactly the same symmetry, when we use LMM with HP, we still have to set $L = \{u_1\}$. The convergence of this numerical solution is slow compared to other solutions. We obtained the numerical eigenfunction u_6 shown in the figure with $\varepsilon < 10^{-2}$. It is interesting to note that u_5 is totally asymmetric even the problem is symmetric and its equivalent class consists of

eight eigenfunctions, and also when we compare the λ-values and their pattern order of of u_2, u_3 in Fig.2.11 with u_3, u_4 in Fig.2.12 and u_3, u_4, u_5 in Fig.2.11 with u_7, u_8, u_9 in Fig.2.12, we see that their λ-values are very close but pattern orders are changed. This is due to the fact that they are actually in different critical point branches of λ so we cannot differentiate them in the order of λ-values. From Figs. 2.11 and 2.12, we also see that $\{\|u_k\|\}$ is bounded for all positive eigenfunctions u_k, which confirms the analysis in Proposition 2.2.1.

By considering the eigen problem on its variational energy profile and using the implicit function theorem, we have developed an implicit minimax method for numerically finding eigenfunctions in the order of their eigenvalues. Its mathematical justification and some interesting properties are established. Note that our problem setting is actually quite general and the theorems proved in this paper can be verified with more general $H(u)$ in other eigen solution problems. However since our main objective of this paper is on computational method and theory on solving nonlinear eigen solution problems not on existence issue, we choose to stay with the original relatively simple $H(u)$ for simpler and clearer presentation of our new idea. Although a Newton method can be used to speed up a local convergence in the above numerical computations, in order to avoid missing variational knowledge (e.g, MI, order, etc.) on the numerical solutions, it should be done after $\varepsilon < 10^{-2}$. Since we want to see the limit of our numerical method, we did not use a Newton method at all in computing the above numerical results.

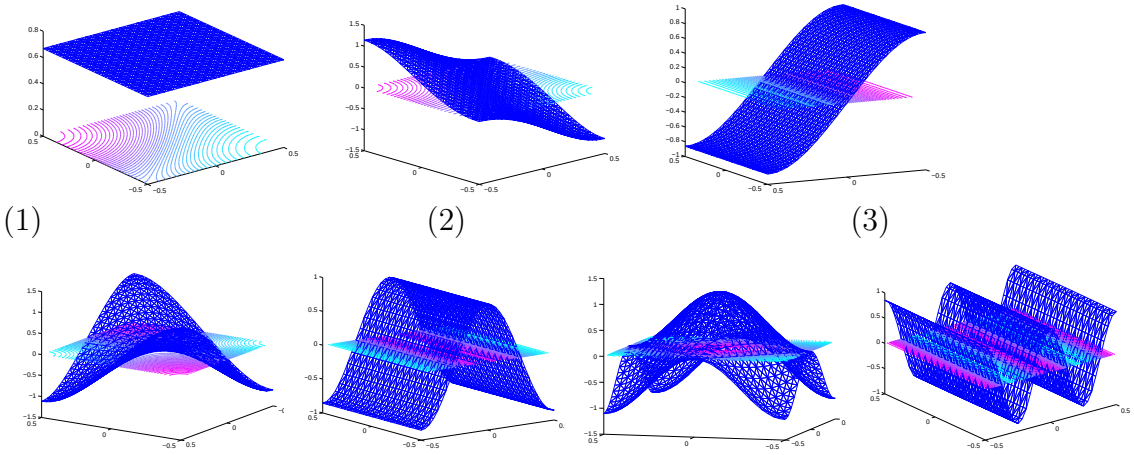

(1) (2) (3)

(4) (5) (6) (7)

Fig. 2.7. $C = 0.25, u_C = 0.6687, \lambda(u_C) = -2.2361$. Profiles and contours of eigenfunctions $u_1, ..., u_7$ with $\lambda(u_i) = -2.2361$, 6.4473, 7.1233, 16.3673, 36.1560, 36.7853, 155.9402 and $\|u_i\|_H = 0.9457$, 1.8468, 2.0748, 2.5229, 3.5020, 3.8904, 7.6583.

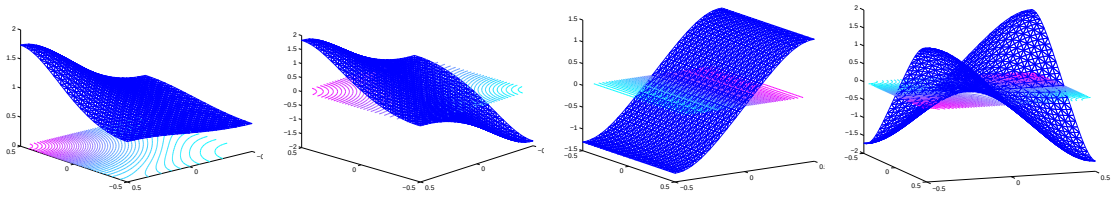

(1) (2) (3) (4)

Fig. 2.8. $C = 1.25, u_C = 1, \lambda(u_C) = -5$. Profiles and contours of eigenfunctions $u_1, ..., u_4$ with $\lambda(u_i) = -5.0308, 1.9666, 3.6925, 12.0753$ and $\|u_i\|_H = 1.6135, 2.7125, 3.0923, 3.7324$.

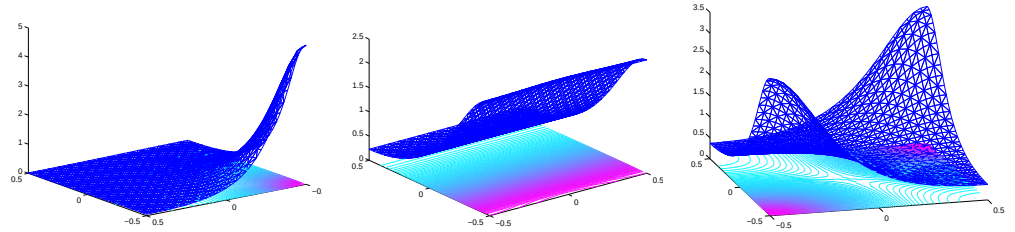

(1) (2) (3) (4)

Fig. 2.9. $C = 7, u_C = 1.5382, \lambda(u_C) = -11.8322$. Profiles and contours of positive eigenfunctions u_1, u_2, u_3 with $\lambda(u_i) = -23.8764, -14.0810, -12.8484$ and $\|u_i\|_H = 3.8876,\ 3.1096,\ 3.6571$.

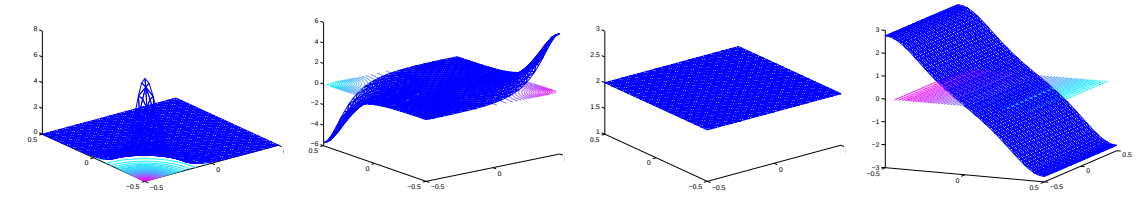

Fig. 2.10. $C = 20, u_C = 2, \lambda(u_C) = -20$. Profiles and contours of eigenfunctions u_1, u_2, u_C, u_4 with $\lambda(u_i) = -67.8699$, -33.9949, -20, -15.6955 and $\|u_i\|_H = 6.3951$, 6.5205, 6.2655,2.8284.

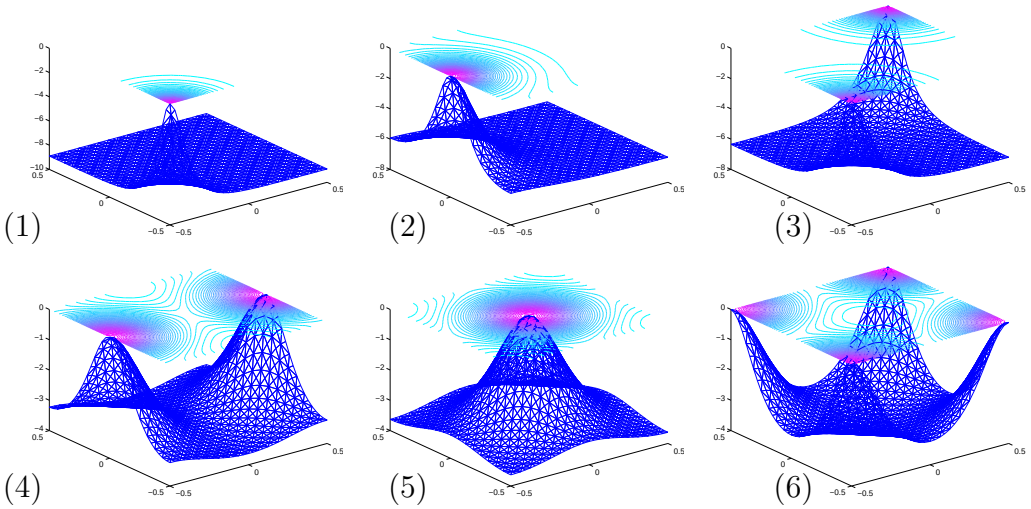

Fig. 2.11. $C = 25, u_C = 2.1147, \lambda(u_C) = -22.3606$. Profiles and contours of positive eigenfunctions $u_1, ..., u_6$ with $\lambda(u_i) = -84.6860$, -42.7914, -42.5634, -23.4976, -23.4976, -23.4976 and $\|u_i\|_H = 7.1234$, 7.1477, 7.2089, 6.2892, 6.2893, 6.2893.

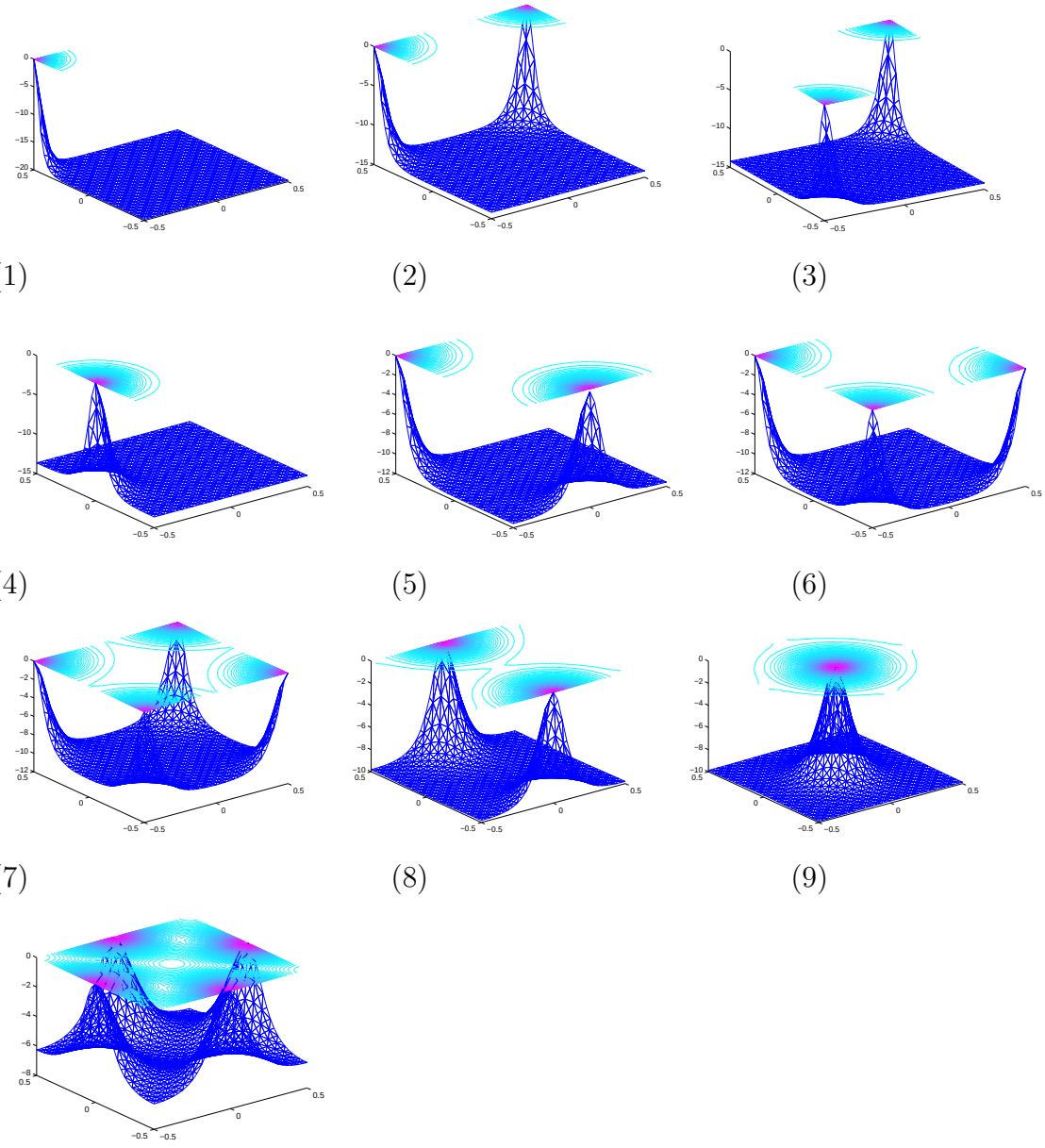

(1) (2) (3)

(4) (5) (6)

(7) (8) (9)

(10)

Fig. 2.12. $C = 125, u_C = 3.1623, \lambda(u_C) = -50$. Profiles and contours of positive eigenfunctions $u_1, ..., u_{10}$ with $\lambda(u_i) = -423.0702, -212.4282, -212.4279, -209.0124, -143.5454, -142.9573, -106.5328, -105.6491, -105.6487, -56.1127$ and $\|u_i\|_H = 15.7391, 15.8416, 15.8416, 15.7213, 15.7097, 15.7737, 15.9291, 15.8651, 15.8651, 14.6269$.

2.3 Application to Defocusing Schrödinger ESP

It is clear that in LMM, the outer is a minimization process that inherits the merit of a minimization method as previously mentioned. The inner level is designed to use the knowledge of some previously found solutions to build a finite-dimensional support L for the outer level to find a new solution.

However when $\kappa < 0$ in (1.9), the defocusing case, the super-quadratic term F brings a very different variational structure to J. Indeed both J and $-J$ have no mountain pass structure. Let us check $-J$ first. Although $-J(tu) \to -\infty$ as $t \to +\infty$ for each $u \neq 0$, but each solution is of infinite Morse index, e.g, $-J''(0) = \Delta + \lambda I$ has infinitely many negative eigenvalues, i.e., $\mathrm{MI}(0) = +\infty$. So the problem becomes infinitely unstable. Consequently an infinite-dimensional support L has to be used in LMM, which causes serious implementation difficulty. So we stay with J and observe that if $\lambda_k < \lambda < \lambda_{k+1}$, then $J(tu) \to +\infty$ as $t \to +\infty$ for each $u \in [u_1, ..., u_k]^{\perp}, u \neq 0$ (W-shaped). So it is clear that LMM cannot be applied. However LMM provides us a hint of using a support L to find multiple solutions.

In this dissertation, we try to use the variational structure of the defocusing NLS to develop certain numerical algorithm for finding multiple solutions in an order.

We note that J is bounded from below, always attains its global minimum and any critical point of J is of finite Morse index, e.g., $\mathrm{MI}(0) = k$ if $\lambda_k < \lambda < \lambda_{k+1}$ since $J''(0) = -\Delta - \lambda I$. Since the super-quadratic term is positive, for each $u \in H$, in order for $J(tu)$ to have a critical point along t at certain $t_u > 0$, we must have

$$\int_\Omega [|\nabla u(x)|^2 - \lambda u^2(x)]dx < 0 \quad \text{and} \quad J(t_u u) < 0. \tag{2.24}$$

So any critical point has a J-value less than 0. The above observation leads to a local max-min principle to characterize solutions:

$$\max_{S_k \subset H} \min_{u \in S_k} J(u) \tag{2.25}$$

where S_k is a subspace of H with co-dimension $k = 0, 1, 2, ...$ Since a local minimum in any subspace exists and their values will be bounded from above by 0, the max-min problem (2.25) is always theoretically and locally solvable. The problem is about its numerical implementation. In this paper we show that when our nonlinear problem possesses certain symmetry, the above two-level max-min method can be simplified to a simple one-level orthogonal subspace minimization method (OSMM) for finding multiple solutions. The basic idea is to use the property that when the problem has certain symmetry, e.g., even or odd symmetric about the origin, the coordinate axes, the lines (plans) $y = x, y = -x$, etc., we use the fact that many different symmetry functional subspaces are orthogonal each other in L^2 and H_0^1 inner products, e.g, the subspace of all even functions and the subspace of all odd functions on Ω. On the other hand, the Rayleigh-Ritz method (RRM) [36], a simple orthogonal subspace minimization problem

$$u_k = \arg \min_{u \in [u_1, ..., u_{k-1}]^\perp} \frac{F(u)}{G(u)}, \ k = 1, 2, ... \tag{2.26}$$

is well-accepted in solving an eigen-solution problem of the form $F'(u) = \lambda G'(u)$ where F', G' are either linear or iso-homogeneous [34]. Note that $[u_1, ..., u_{k-1}]^\perp$ is an orthogonal subspace to $[u_1, ..., u_{k-1}]$ with co-dimension $k - 1$. So RRM simplifies the max-min characterization (2.25). But it will, in general, not work for nonlinear problems.

Here we devise OSMM by modifying RRM for finding multiple solutions to the *defocusing* problem (1.9) with $\kappa < 0$. We first provide some mathematical background and description of our new method and then we describe how we resolve an important numerical implementation issue, i.e., how we remove the part of a numerical error sensitive to our algorithm search by a projection to an infinite dimensional subspace. This is vitally important since we are searching for unstable solutions. We will carry out some numerical examples and display our numerical results by their profile and contour plots for visualization.

2.3.1 An orthogonal subspace minimization method

Let $L \subset$ be a closed subspace in H and u^* be a local minimum point of J restricted to $L^\perp$. So $\nabla J(u^*) \perp L^\perp$ or $\nabla J(u^*) \in L$. But there is no guarantee that $\nabla J(u^*) = 0$. So it will not work for a critical point. In order for RRM or our OSMM to work, we need to use the symmetry of the problem, a very common property for many application problems in physics. To show the mathematical background of our new approach, let us introduce two simple theorems.

Theorem 2.3.1 *Let H be a Hilbert space, $J \in \mathcal{C}^1(H, \mathbb{R})$ and $S \subset H$ be a closed subspace such that $\nabla J : S \to S$. If u^* is a critical point of J restricted to S, then u^* is a critical point of J in H.*

Proof If $u^* \in S$ is a critical point J restricted to S, then $\nabla J(u^*) \perp S$. Since $\nabla J(u^*) \in S$, we conclude $\nabla J(u^*) = 0$. ■

How to choose a subspace $S \subset H$ s.t. $\nabla J : S \to S$? From [25,26], let G be a compact group of actions (linear isometrically) on H and S_G be the symmetry invariant subspace defined by G, i.e., $u \in S_G$ if and only if $gu = u \; \forall g \in G$. Then J is G-invariant, i.e., $J(gu) = J(u)$ for all $u \in H, g \in G$, implies that $\nabla J(u) \in S_G, \forall u \in S_G$. By Theorem 2.3.1, we have the well-known (Principle of Symmetric Criticality, Palais, 1979) [25]:

Theorem 2.3.2 *Let H be a Hilbert space and G be a compact group of actions on H and $J \in \mathcal{C}^1(H, \mathbb{R})$ be G-invariant. If u^* is a critical point of J restricted to S_G, then u^* is a critical point of J in H.*

So theoretically a critical point can be found by a gradient method as a local minimum point of J restricted to S_G in four steps:

Step 1: Given $\varepsilon > 0$, initial guess $u_0 \in S_G$. Set $k = 0$;

Step 2: Compute $d_k = \nabla J(u_k)$. If $\|d_k\| < \varepsilon$, then output u_k and stop; else go to Step 3;

Step 3: Set $u_{k+1} = u_k - s_k d_k \in S_G$ where $s_k > 0$ satisfies the Armijo's stepsize rule:

$$J(u_{k+1}) - J(u_k) < -\frac{1}{2}\|d_k\|^2; \tag{2.27}$$

Step 4: Set $k = k + 1$ and goto Step 2.

Theoretically the above algorithm is symmetry invariant and its convergence, with the Armijo's stepsize rule, can be easily established if we do not consider any numerical error. So we obtain a critical point $u^* \in S_G$. Motivated by LMM and RRM, we can also introduce a support L to find multiple critical points in an order as described in the following flow chart:

Step 0: Given $\varepsilon > 0$. Set $w_0 = 0, n = 1$;

Step 1: Set $L = [w_1, ..., w_{n-1}]$ where $w_1, ..., w_{n-1}$ be previously found solutions. Choose a maximum symmetry invariant subspace $S_G \subset L^\perp = [w_1, ..., w_{n-1}]^\perp$ and select an initial guess $u_0 \in S_G$. Set $k = 0$;

Step 2: Compute $d_k = \nabla J(u_k)$. If $\|d_k\| < \varepsilon$, then output $w_n = u_k, n = n + 1$ goto Step 1 else go to Step 3;

Step 3: Set $u_{k+1} = u_k - s_k d_k \in S_G$ where $s_k > 0$ satisfies the Armijo's stepsize rule (2.27);

Step 4: Set $k = k + 1$ and goto Step 2.

So every time if the algorithm is successful, a new solution $w_n \in L^\perp$ is found and it is clear that we have $J(w_k) \leq J(w_n), k < n$. The algorithm seems very simple, but actually contains a serious problem in its implementation due to numerical error in

finding an unstable saddle point or a local minimum point in a subspace not in H, since the algorithm did not enforce the symmetry.

To address this issue, let e_k denote the numerical error in approximating $\nabla J(u_k) \in S_G$ where $u_k \in S_G$ and $d_k = \nabla J(u_k) + e_k$. In general, $e_k \notin S_G$ even e_k is small in norm. Without enforcing the symmetry, it leads to the search direction $d_k \notin S_G$ and then $u_{k+1} \notin S_G$. Once the symmetry is broken, the symmetry invariance of the algorithm collapses and the algorithm is no longer self-contained in the subspace S_G. If we look for a local minimum point in H, then there is no problem with such error since $e_k \in H$ anyway. Even the symmetry is broken, the minimizer search still leads to a local minimum point in H. But if we look for a saddle point which is a local minimum of J in a subspace S_G not in H, once the symmetry invariance of the algorithm is broken, the minimizer search may sense a descent direction outside S_G and follow it to a point outside S_G with a smaller J-value. So this part of error will be significantly increased and eventually lead to a local minimum point outside S_G, an unwanted solution. The Haar projection of d_k onto S_G can be used to enforce the symmetry on d_k [25]. But when a symmetry is very complex or unknown, the Haar projection becomes much more complex or impossible. In particular, if a finite element mesh used in a computation does not match the symmetry, then it is impossible to do the Haar projection. So far the literature does not provide any alternative. Next we propose a new method to handle such numerical error.

2.3.2 Removal of sensitive error in numerical implementation

The basic idea of the new method consists of two parts:

(1) when a minimizer search is concerned, the space H can be divided into two portions: its "lower portion" which contains critical points with smaller J- values, denoted by L and also called a support and its complement $L^{\perp}$ called "upper portion" which contains critical points with larger J-values. When descent directions into the "lower portion" are blocked, the minimizer search leads to a local minimum point

w^* in the "upper portion" $L^\perp$. But in general this local minimum point w^* in the "upper portion" need not be a critical point since $P_L(\nabla J(w^*)) = 0$ but not necessarily $P_{L^\perp}(\nabla J(w^*)) = 0$ where P_L and $P_{L^\perp}$ are respectively the linear projections onto L and $L^\perp$;

(2) Select a maximum symmetry invariant subspace (MSIS) $S_G \subset L^\perp$ and choose an initial guess $u_0 \in S_G$. In the above minimizer search, we partition the numerical error e_k into $e_k = e_k^L + e_k^\perp$ where $e_k^L \in L, e_k^\perp \in L^\perp$. Since a minimizer search is attracted only to the part e_k^L in the "lower portion" and may lead to much smaller J-values, not attracted to the part $e_k^\perp$ in the "upper portion". So to get rid of e_k^L, we modify $\bar{d}_k = \nabla J(u_k)$ by an orthogonal projection d_k of $\bar{d}_k$ onto the infinite-dimensional subspace $L^\perp$ and do

$$d_k = \bar{d}_k - P_L(\bar{d}_k)$$

where $P_L(\bar{d}_k)$ is the projection of $\bar{d}_k$ onto the finite-dimensional space L. Since the part of numerical error $e_k^\perp \in L^\perp$ is not attractive to a minimizer search and is dominated by $\nabla J(u_k) \in S_G \subset L^\perp$, $e_k^\perp$ will not be enlarged and the approximation sequence $\{u_k\}$ stays close to S_G. Consequently, the minimizer search finds an approximation of a local minimum point $w^* \in S_G \subset L^\perp$ of J restricted to $L^\perp$. So $P_{L^\perp}(\nabla J(w^*)) = 0$. On the other hand since $w^* \in S_G$ implies $\nabla J(w^*) \in S_G \subset L^\perp$, we conclude $\nabla J(w^*) = P_{L^\perp}(\nabla J(w^*)) = 0$, i.e., $w^* \in S_G \subset L^\perp$ is a critical point of J.

It leads to the following flow chart of an orthogonal subspace minimization method (OSMM)

Step 0: Given $\varepsilon > 0$. Set $w_0 = 0, n = 1$;

Step 1: Set a support $L = [w_1, ..., w_{n-1}]$ in the "lower portion" where $w_1, ..., w_{n-1}$ are of previously found solutions. Identify a MSIS $S_G \subset L^\perp = [w_1, ..., w_{n-1}]^\perp$ and select an initial guess $u_0 \in S_G$. Set $k = 0$;

Step 2: Compute $d_k = \nabla J(u_k)$. If $n > 1$, do $d_k = d_k - P_L(d_k)$. If $\|d_k\| < \varepsilon$, then output $w_n = u_k, n = n + 1$ goto Step 1 else go to Step 3;

Step 3: Set $u_{k+1} = u_k - s_k d_k \in S_G$ where $s_k > 0$ satisfies the Armijo's stepsize rule (2.27);

Step 4: Set $k = k + 1$ and goto Step 2.

Remark 2.3.1 (1) To identify a MSIS S_G, since it may not be unique. one should choose an initial guess in S_G accordingly. Consequently it may lead to multiple solutions branches;

(2) So one branch may bifurcate to two or more branches, and on the other hand, two or more branches may merge to one branch. This is the complexity that one has to face with multiple solution problems. When multiple branches of solutions exist, one should choose those previously found solutions accordingly to form L;

(3) Since we do not enforce a symmetry, a MSIS is invisible and selected only by the symmetry of an initial guess. Even a selected initial guess is actually in a smaller symmetry invariant subspace $S_{G'} \subset S_G$, the algorithm will still lead to a critical point in a MSIS S_G. To see this we write $e_k^{\perp} = e_k^G + e_k'$ where $e_k' \in L^{\perp} \setminus S_G$ is dominated by $\nabla J(u_k)$ and $e_k^G \in S_G$ is kept in the algorithm, which attracts the minimizer search and helps it to find a local minimum point w^* in $S_G \setminus S_{G'}$. Note that in this case, there will also be a local minimum point in $S_{G'}$ which is at an upper energy level of w^*. It means that the subspace L is not a maximum "lower portion" of the minimizer search in $S_{G'}$, so it is not enough to support the minimizer search to find a local minimum point in $S_{G'}$;

(4) There is only one problem left, that is, what should we do if $e_k^{\perp}$ is not dominated by $\nabla J(u_k)$? There are two alternatives:

(a) The numerical error $e_k^{\perp}$ is small and $\nabla J(u_k)$ is smaller. That means u_k is already a good approximation of a critical point. We may simply stop the iteration and output u_k, or switch to a Newton method to accelerate the local convergence;

(b) The numerical error $e_k^{\perp}$ is not small but $\nabla J(u_k)$ is small. Then we either reduce the numerical error by using a symmetric mesh that matches with the symmetry of the problem or switch to a Newton method that speeds up local convergence, since a Newton method is insensitive to such numerical error [26].

A more detailed example will be presented in the last section to show how to identify a MSIS $S_G \subset L^{\perp}$ in a numerical computation.

(5) For MI(w_n), since in OSMM, the minimizer search is in a MSIS S_G in the subspace $L^{\perp} = [w_1, ..., w_{n-1}]^{\perp}$ but we do not enforce symmetry and allow $e_k^L \in L^{\perp}$ to exist, we cannot obtain a precise Morse index estimate as in Theorem 2.2.2. However, if $\text{codim}(S_G) = k \geq n-1$ and $\{w_1, ..., w_{n-1}\}$ are in the same critical branch, then we should have $n-1 \leq \text{MI}(w_n) \leq k$ and $\text{MI}(w_i) \leq \text{MI}(w_n), J(w_i) < J(w_n), i = 1, ..., n-1$. So solutions are solved in this order. But this order is not complete if $w_1, ..., w_n$ are not in the same critical branch. For example, with $L = [w_1]$, by using two different MSIS S_G and two different initial guesses in S_G, we may find two different solutions w_2^1, w_2^2 with $J(w_1) < J(w_2^i)$ and $\text{MI}(w_2^i) = 2, i = 1, 2$. But we cannot compare $J(w_2^1)$ with $J(w_2^2)$.

One may ask why can't we use a Newton method at the very beginning? In addition to the reasons mentioned in the introduction, there is another one, i.e., the invariance of a Newton method to symmetries and this invariance is also insensitive to numerical error [26]. So a Newton method may be easily trapped in a symmetry invariant subspace defined by an initial guess but different from that of a target solution. Note that $u = 0$ is a critical point in any symmetry invariant subspace. This means that even the symmetry of an initial guess is selected correctly, it still needs to be scaled for a Newton method to stay away from the local basin of $u = 0$. Without using a variational structure, it is hard to determine this scale.

Numerical results

In this section we apply OSMM developed in the previous sections to find multiple solutions first to (1.9) with some fixed λ value which is a defocusing PDE problem and then to (1.9) as an ESP for several typical cases. We use a symmetric finite element mesh as Fig. 2.13 (1) or its locally refined mesh such as Fig. 2.14 (1) so that the equation and the energy functional J satisfy all symmetry invariant property. Since NLS (1.8) is defined in the entire space while equation (1.9) is defined in a bounded open domain, for (1.9) to be valid, its solutions must have a localized property. So we will closely check this property through solution contour plots with several different external trapping potential $v(x)$. In order to clearly plot a profile and its contours in one figure we have shifted the profile vertically in the figure.

Example 2.3.1 (An autonomous defocusing case) In (1.9), we choose $f(x, |u|)u(x) = u^3(x)$, $\kappa = 1, \lambda = 200$, $\Omega = (-0.5, 0.5)^2$ and $\varepsilon = 10^{-4}$. For each fixed λ, there are only finite number of solutions. Then the algorithm can be described in detail as below:

1. The algorithm starts from $L = \{0\}$, $S_G = H, u_0 \in H$ be any nonzero function. Denote the solution by w_1 that is a positive and even symmetric function about the lines $x = 0, y = 0, y = x, y = -x$;

2. Then we set $L = [w_1]$, denote MSIS S_G the set of all odd functions about one of the lines $x = 0, y = 0, y = x, y = -x$. It is clear that $S_G \subset L^{\perp}$. So choose $u_0 \in S_G$. Denote the solution by w_2 which is odd symmetric about one of the four lines. Note that there are multiple solutions here due to different initial guess that is odd symmetric about a different line of the four. But their Morse index should be the same;

3. Next we set $L = [w_1, w_2]$, denote MSIS S_G a smaller subspace of odd functions about two lines, e.g. $x = 0$ and $y = 0$ or $y = x$ and $y = -x$. It is clear that

$S_G \subset L^\perp$. Choose $u_0 \in S_G$. Denote the solution by w_3 that is odd symmetric about the two lines of symmetry. Note that there may be multiple solutions due to different initial guess, which may lead to multiple branches. But their Morse index should be the same;

4. Continue in this way. Note that in order to find a solution with higher Morse index, we may need put more previously found solutions in the support L;

5. The above algorithm finds a local minimum of J in the subspace $L^\perp$. The MSIS S_G is only an invisiable bridge not enforced. When an initial guess u_0 is chosen in a smaller symmetry invariant subspace (means more symmetric), due to computational error e_k, the above algorithm will leads to a solution in a MSIS in $L^\perp$.

At each point u_k, $d_k = \nabla J(u_k)$ is evaluated through solving a linear elliptic PDE of the form

$$-\Delta d_k(x) + \lambda d_k(x) = -\Delta u_k(x) + \lambda u_k(x) - \kappa F(x, u_k(x))$$

satisfying zero Dirichlet boundary condition. There are many numerical methods available in the literature to solve such a problem. This is where a numerical error is generated. We use a finite element method by calling Matlab subroutine ASSEMPDE. A symmetric finite element mesh is generated by Matlab mesh generator INITMESH and REFINEMESH, and shown in Fig. 2.13 (1).

The first 7 numerical solutions $u_1, ..., u_7$ are shown in Fig. 2.13 (2)$\sim$(8). Their energy values $J(u_i) = -5,290.6$; $-3,262.3$; $-3,262.3$; $-2,886.3$; $-2,886.3$; $-1,853.9$; $-1,153.0$; their norms $\|u_i\| = 63.7635$, 73.6002, 73.6002, 71.4513, 71.4513, 74.1284, 69.2141 and their supports $L = [0]$, $[u_1]$, $[u_1]$, $[u_1]$, $[u_1]$, $[u_1, u_2, u_3]$, $[u_1, u_4, u_5]$. We have also solved the same problem with larger domains and different λ values. Since the external trapping potential $v = 0$, all their solution profiles do not show a localized property.

In our numerical computation, we have tried to use: (1) a more symmetric initial guess in $L^{\perp}$, it leads to a less symmetric solution in $L^{\perp}$; (2) asymmetric initial guesses in $L^{\perp}$, it is amazing that as long as the support L is sufficient they still lead to those solutions. But we are not able to establish any mathematical justification for such cases so far.

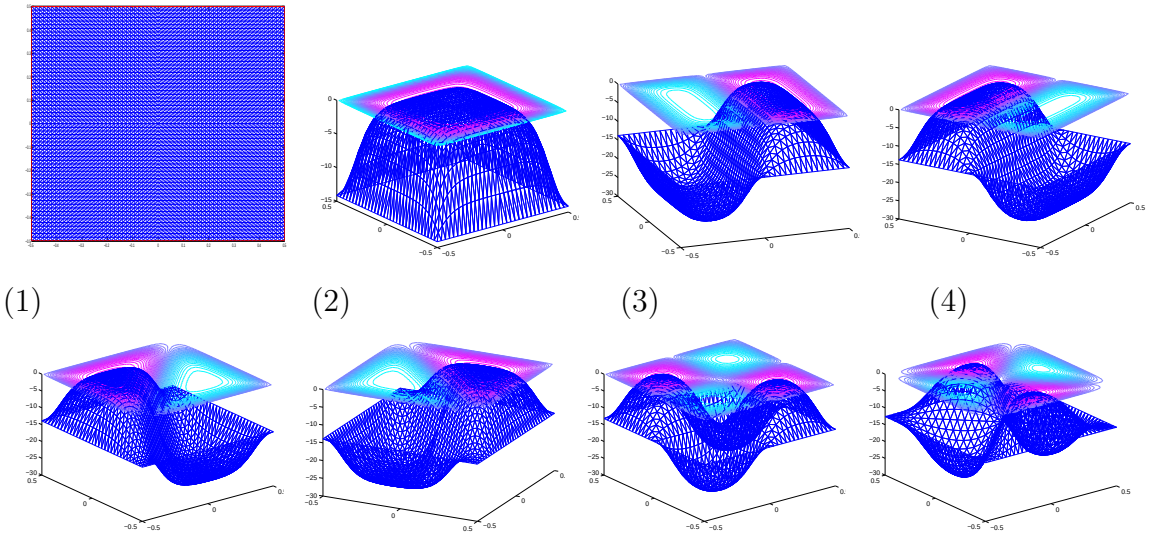

Fig. 2.13. A typical symmetric finite element mesh (1). The first 7 numerical solutions $u_1, ..., u_7$ in (2)$\sim$(8), to Example 2.3.1. The contours show that the solutions are not localized.

Example 2.3.2 (A non-autonomous defocusing case) In (1.9), we choose $f(x, |u|)u = |x|^r u^3(x)$ with $r = 3$, $\kappa = -1, \lambda = 100$, $\Omega = (-1, 1)^2$ and $\varepsilon = 10^{-4}$.

The first 6 numerical solutions $u_1, ..., u_6$ are shown in Fig. 2.14 (2)$\sim$(7). Their energy values $J(u_i) = -130,550;\ -32,737;\ -32,737;\ -32,286;\ -32,286;\ -13,206$; the norms of their solution $\|u_i\|^2 = 389.4356$, 224.2219,224.2219, 225.5204, 225.5201, 173.1593 and their supports $L = [0]$, $[u_1]$, $[u_1]$, $[u_1]$, $[u_1]$, $[u_1, u_2, u_3], [u_1, u_4, u_5]$. We note that solution peaks are sharp, narrow and very close. To compute a sign-changing solution, evenly meshed finite elements lost their accuracy, so local mesh

refinements in a small region near the center $(0,0)$ have to be used to maintain our computational accuracy. A locally refined finite element mesh generated by Matlab mesh generator INITMESH and REFINEMESH is shown in Fig 2.14 (1). Though the peaks are sharp and narrow, the solutions look like localized, but are actually not since their contours still spread out all over the domain. We also note that there is no symmetry breaking taken place, which is in contrast to its focusing counterpart such as the Henon equation.

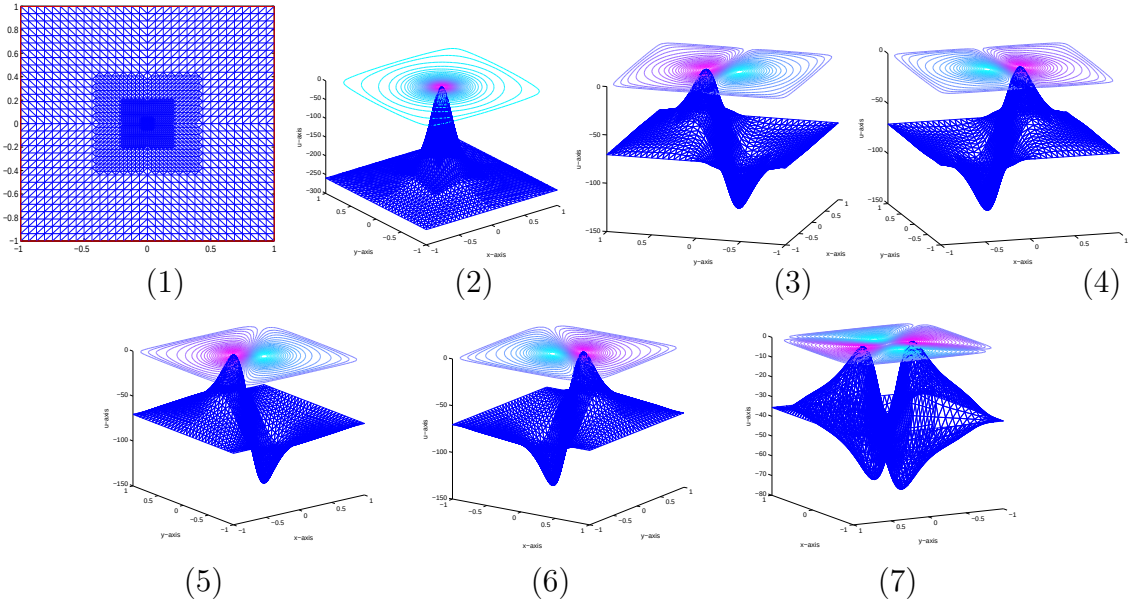

Fig. 2.14. A typical locally refined finite element mesh (1). The first 6 numerical solutions $u_1, ..., u_6$ in (2)$\sim$(7) to Example 2.3.2.

Example 2.3.3 (A defocusing case with a symmetric external trapping potential) In (1.9) we choose a nonzero symmetric external trap potential $v(x) = r|x|^2, r = 200$, $\kappa = -1$, $\lambda = 100$, $f(x,|u(x)|)u(x) = u^3(x)$, $\Omega = (-1,1)^2$ and $\varepsilon = 10^{-4}$. The variational energy of u is

$$J(u) = \int_\Omega \{\frac{1}{2}[v(x) - \lambda]u^2(x) + \frac{1}{2}|\nabla u(x)|^2 + \frac{1}{4}u^4(x)\}dx.$$

So for $u \in H$ to be a solution, we must have

$$\int_{\Omega} [v(x) - \lambda] u^2(x) dx < 0, \tag{2.28}$$

which will force the peaks of u to concentrate on an area where $v(x)$ is small. We note that when r is larger or λ is smaller, inequality (2.28) will force the peaks of u to concentrate on a smaller area where $v(x)$ is smaller. So the solution peaks are localized in the area. For each λ, there are only finite number of solutions. The first 7 numerical solutions $u_1, ..., u_7$ are shown in Fig. 2.15. Their energy values $J(u_i) = -1,046.0$; -412.0963; -412.0963; -410.896; -410.896; -57.8304; -56.439; their solution norms $\|u_i\| = 20.695$,28.2988,28.2988,28.363, 28.363,23.2704,23.3154 and their supports $L = [0], [u_1]$, $[u_1]$, $[u_1], [u_1]$, $[u_1, u_2, u_3]$, $[u_1, u_4, u_5]$. The solution contours show a clear localized property.

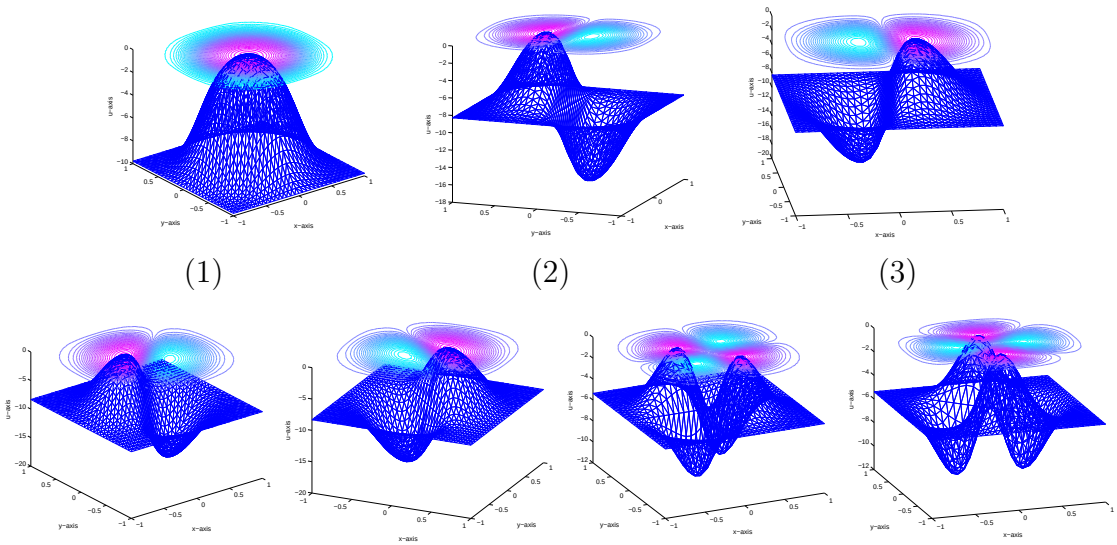

Fig. 2.15. The first 7 numerical solutions $u_1, ..., u_7$ to Example 2.3.3. The solutions are localized.

Example 2.3.4 (A defocusing case with a less symmetric external trapping potential) To show that our method works for problems with less symmetry, in (1.9), we choose all the same parameters as in Example 2.3.3 except a less symmetric external trapping potential $v(x) = r(\frac{2}{3}x_2 + \frac{4}{3}x_2^2), r = 200$. So for $u \in H$ to be a solution, the inequality (2.28) will force the peaks of u to concentrate on an elliptical area where $v(x)$ is smaller. So the localized property should also be observed. This analysis is confirmed by our numerical computation. The first 4 numerical solutions $u_1, ..., u_4$ are shown in Fig. 2.16. Their energies $J(u_i) = -1.1283e+3, -645.3762, -268.2216, -59.8842$, their solution norms $\|u_i\| = 23.2462$, 29.4751, 29.2566, 24.0469 and their supports $L = [0], [u_1], [u_1], [u_1, u_2, u_3]$.

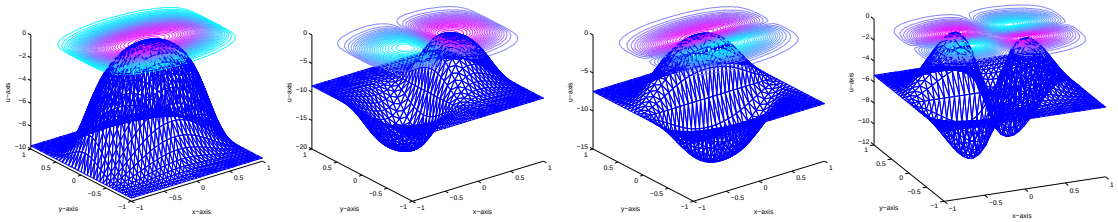

(1) (2) (3) (4)

Fig. 2.16. The profiles of the first 4 numerical solutions $u_1, ..., u_4$ for Example 2.3.4.

Example 2.3.5 As a last example to PDE (1.9), we choose $v(x) = r(\sin^2(2\pi x_1) + \sin^2(2\pi x_2))$ with $r = 100$ and other terms remain the same as in Example 2.3.3.

The first 7 numerical solutions $u_1, ..., u_7$ are shown in Fig. 2.17 with their energy values $J(u_i) = -764.4081, -460.3365, -460.3365, -454.8088, -454.8088, -250.1220, -229.2876$, their norms
$\|u_i\| = 44.0352, 37.7503, 37.7503, 37.7907, 37.7907, 32.2368, 32.5469$ and their supports $L = [0], [u_1], [u_1], [u_1], [u_1], [u_1, u_2, u_3], [u_1, u_4, u_5]$. The solution profiles show an interesting phenomenon i.e., *higher order (MI) solutions have less peaks, a significant contrast to all previous examples.*

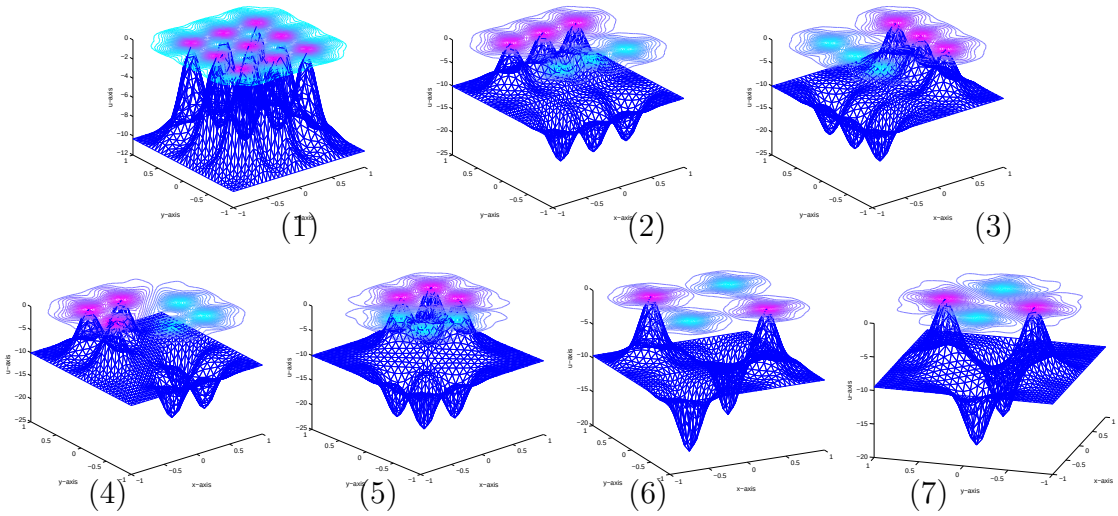

Fig. 2.17. The profiles of the first 7 numerical solutions $u_1, ..., u_7$ to Example 2.3.5.

Example 2.3.6 (A defocusing ESP without external trapping potential) Next we solve the defocusing ESP (1.9) for multiple solutions (λ, u). We choose $v(x) = 0, \kappa = -1$, $f(x, u(x))u(x) = u^3(x)$, $\Omega = (-0.5, 0.5)^2$ and $\varepsilon = 10^{-4}$, $C = 900$ and $C = 10$, and want to see the shape difference between the eigen functions at different energy levels.

The first 8 numerical eigen functions $u_1, ..., u_8$ at the energy level $-C = -900$ are shown in Fig. 2.18 with eigenvalues $\lambda_i = 98.8414$, 131.6574, 131.6574, 137.3578, 137.3578, 164.7840, 190.5393, 292.7556, their norms $\|u_i\| = 35.0447$, 49.9499, 49.9499, 49.3652, 49.3652, 60.1673, 65.3372, 88.2909 and their supports $L = [0]$, $[u_1]$, $[u_1]$, $[u_1]$, $[u_1]$, $[u_1, u_2, u_3]$, $[u_1, u_4, u_5]$, $[u_1, u_4, u_5, u_6, u_7]$.

The first 8 numerical eigen functions $u_1, ..., u_8$ at the energy level $-C = -10$ are shown in Fig. 2.19 with eigenvalues $\lambda_i = 28.9900$, 58.7792, 58.7792, 59.5321, 59.5321, 88.6519, 109.1362, 208.8727, their norms $\|u_i\| = 9.3864, 14.6748$, 14.6748, 14.1167, $14.1167, 18.4019$, $19.8152, 27.4468$ and their supports $L = [0], [u_1]$, $[u_1]$, $[u_1]$, $[u_1]$, $[u_1, u_2, u_3]$, $[u_1, u_4, u_5]$, $[u_1, u_4, u_5, u_6, u_7]$.

Compare those two cases, we see that the tops of solution peaks are more flat when C is larger. From their contour plots we see that such eigen functions do not show a localized property, because the external trapping potential $v(x) = 0$.

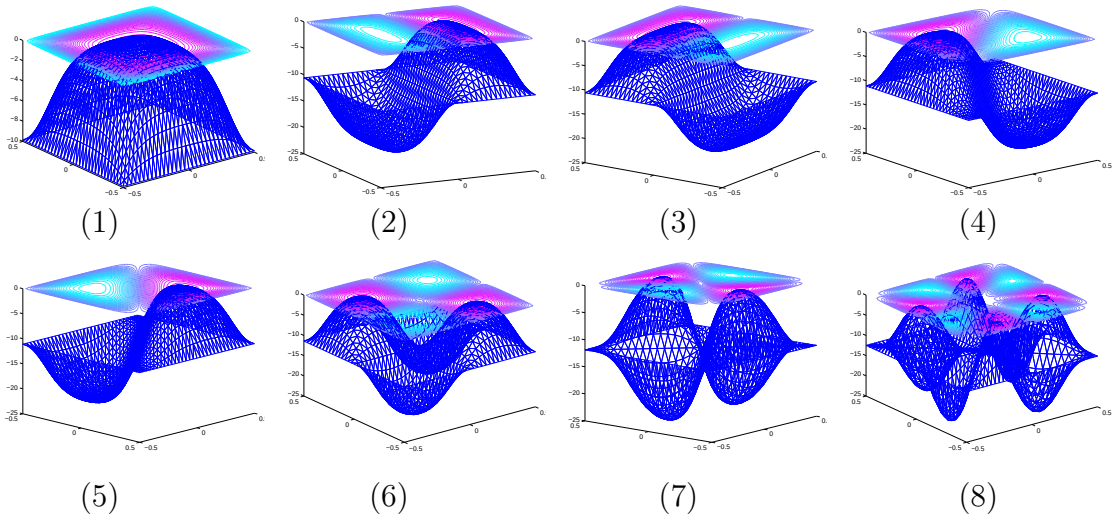

Fig. 2.18. The profiles of the first 8 numerical eigen functions $u_1, ..., u_8$ for Example 2.3.6 with $v(x) = 0$ at the energy level $-C = -900$. The contours show that the eigen functions are not localized.

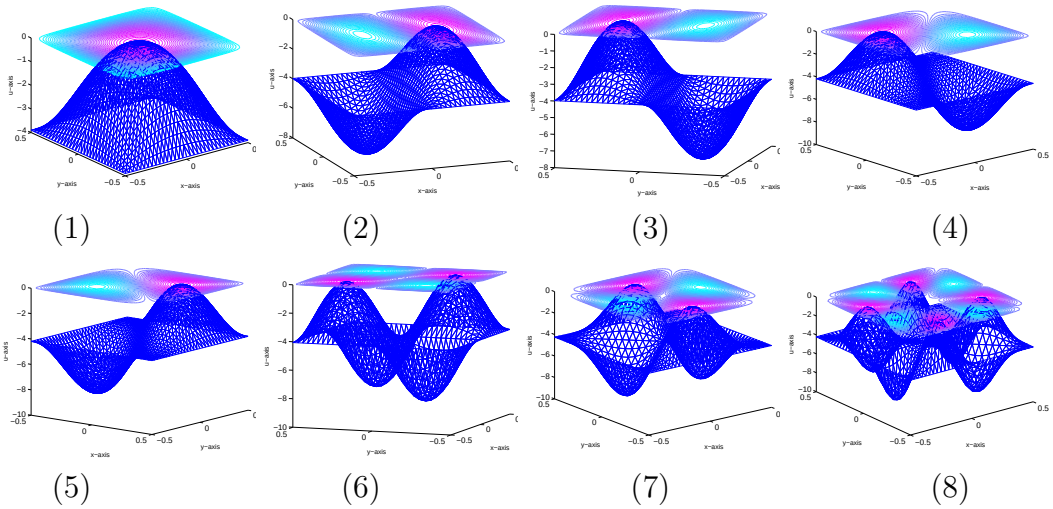

Fig. 2.19. The first 8 numerical eigen functions $u_1, ..., u_8$ for Example 2.3.6 with $v(x) = 0$ at the energy level $-C = -10$. The contours show that the eigen functions are not localized.

Example 2.3.7 (A defocusing eigen problem with external trapping potential) We choose $v(x) = r(x_1^2 + x_2^2)$ with $r = 200$ at the energy level $-C = -900$. All other parameters remain the same as in Example 2.3.6. So the potential function is symmetric. We have

$$\lambda(u) = \frac{F(u) + C}{G(u)} = \frac{\int_\Omega [|\nabla u(x)|^2 + v(x)u^2(x) + \frac{1}{2}u^4(x)]dx + 2C}{\|u\|_{L^2}^2}.$$

It has the same symmetric property as that of λ in Example 2.3.6 with $v(x) = 0$. So our method can be applied to find its multiple eigen solutions. The first 8 numerical eigen functions are shown in Fig. 2.20 with eigenvalues $\lambda_i = 96.6997$, 118.4102, $118.4102, 118.4792$, 118.4792, 142.9253, 143.2324, 195.1539, their norms $\|u_i\| = 19.9896$, 34.9773, 34.9773, 35.1204, 35.1204, 47.3457, 47.9260, 68.4491 and their supports $L = [0], [u_1], [u_1]$, $[u_1], [u_1]$, $[u_1, u_2, u_3]$, $[u_1, u_4, u_5], [u_1, u_4, u_5, u_6, u_7]$. Their contour plots show a clear localized property.

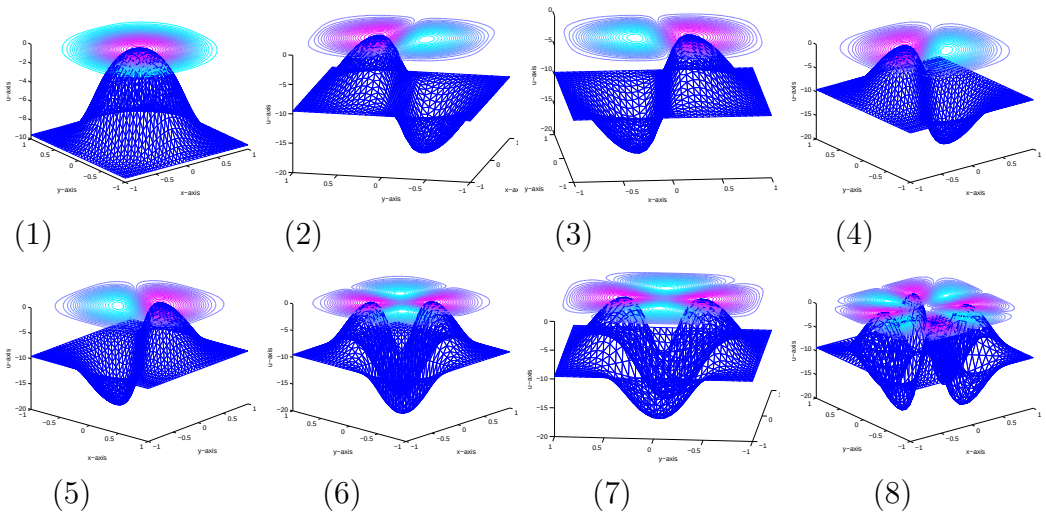

Fig. 2.20. The first 8 numerical eigen functions $u_1, ..., u_8$ for Example 2.3.7 with $v(x) = 200(x_1^2 + x_2^2)$ at the energy level $-C = -900$. The contours show a clear localized property.

3. SEMI-LINEAR ELLIPTIC SYSTEM WITHOUT A COMMON VARIATIONAL FORM

In this chapter we discuss the semi-linear elliptic system (1.15) where $W^1(u(x), v(x))$ and $W^2(u(x), v(x))$ in (1.16) are not proportional. A new joint local min orthogonal method is developed to numerically solve the problem for multiple solutions.

3.1 A Joint Local Min Orthogonal Method for Systems

In [40,42] a local min max orthogonal method(LMMOM) has been developed to solve cooperative/noncooperative nonlinear elliptic system. The method possesses some good properties that it can find multiple solution in the order of variational energy, it can generally find new solutions and does not highly rely on initial guesses by using the support spanned by previously found solutions, and last but not least it can deal with degenerate cases.

Although the method can not be used for solving our problem since the variational form of the system is not available, we want to develop a new method motivated by the idea of LMMOM and hope that the new method still gains those good properties.

First we need create a new solution characterization, the local joint orthogonal characterization. Throughout this chapter, we use the following notations. For $i = 1, 2$, let H_i be a Hilbert Space with inner product $\langle \cdot, \cdot \rangle$ and norm $\| \cdot \|$. Let L_i be a closed subspace of H_i and $L_i \oplus L_i^{\perp}$ be an orthogonal decomposition of H_i. Denote $H = H_1 \times H_2$, $L = L_1 \times L_2$ and $L^{\perp} = L_1^{\perp} \times L_2^{\perp}$. Denote $\tilde{S}_B = \{v \in B \mid \|v\| = 1\}$ for any subspace B of H_i and $S_{L^{\perp}} = \tilde{S}_{L_1^{\perp}} \oplus \tilde{S}_{L_2^{\perp}} \subset L^{\perp}$. Assume that F, G are in $\mathcal{C}^1(H, \mathbb{R})$, and $(F_u(u, v), F_v(u, v))$, $(G_u(u, v), G_v(u, v))$ are their gradients.

Definition 3.1.1 *The set-valued mapping $P : S_L^{\perp} \to 2^H$ is the joint orthogonal mapping of $(F(u, v), G(u, v))$ if for each $w = (w_1, w_2) \in S_{L^{\perp}}$*

$$P(w) = \{(u, v) \in [L_1, w_1] \times [L_2, w_2] : F_u(u, v) \perp [L_1, w_1], G_v(u, v) \perp [L_2, w_2]\}. \tag{3.1}$$

Definition 3.1.2 *A single valued mapping p: $S_{L^\perp} \to H$ is called a joint orthogonal selection of $(F(u,v), G(u,v))$ if $p(w) \in P(w)$. For a given $w^0 \in S_{L^\perp}$ if $p(w)$ is locally defined in $\mathcal{N}(w^0) \cap S_{L^\perp}$ where $\mathcal{N}(w^0)$ is a neighborhood of w^0, then $p(w)$ is called a local joint orthogonal selection of (F_u, G_v) at w^0.*

Lemma 3.1.1 *[33] For any unit vector x_1 in a Hilbert space $(X, \|\cdot\|)$, we have that*

$$\frac{\|x\|}{\|x_1 \pm x\|} \leq \|\frac{x_1 \pm x}{\|x_1 \pm x\|} - x_1\| \leq \frac{2\|x\|}{\|x_1 \pm x\|}, \forall x \in X \quad with \quad x \perp x_1. \tag{3.2}$$

The following theorem is very important for establishing a local characterization of solutions to (1.16) and a step-size rule of JLMOM.

Theorem 3.1.1 *Suppose that F, G are in $\mathcal{C}^1(H, \mathbb{R})$, L is a closed subspace of H, $w = (w_1, w_2) \in S_{L^\perp}$, $p(w)$ is a joint orthogonal selection of $(F(u,v), G(u,v))$ at w. Denote $p(w) = (p_1(w), p_2(w)) = (t_1 w_1 + l_1, t_2 w_2 + l_2)$ with $t_1 t_2 \neq 0$, $(l_1, l_2) \in L$, $d_1 = F_u(p(w))$, $d_2 = G_v(p(w))$ and $w_1(s_1) = \frac{w_1 - sign(t_1) s_1 d_1}{\|w_1 - sign(t_1) s_1 d_1\|}$, $w_2(s_2) = \frac{w_2 - sign(t_2) s_2 d_2}{\|w_2 - sign(t_2) s_2 d_2\|}$. If p is continuous at w then $\exists s_0$, s.t.*

$$\begin{aligned} & F(p_1(w_1(s_1), w_2(s_2)), p_2(w_1, w_2)) - F(p(w_1, w_2))) \\ < \; & -\frac{1}{4} s_1 \cdot |t_1| \|d_1\|^2, \quad if \; \|d_1\| > 0, \end{aligned} \tag{3.3}$$

$$\begin{aligned} & G(p_1(w_1, w_2)), p_2(w_1(s_1), w_2(s_2))) - G(p(w_1, w_2))) \\ < \; & -\frac{1}{4} s_2 \cdot |t_2| \|d_2\|^2, \quad if \; \|d_2\| > 0 \end{aligned} \tag{3.4}$$

for $0 < s_1, s_2 < s_0$.

Proof By continuity, $(w_1(s_1), w_2(s_2)) \to (w_1, w_2)$ as $s_1 \to 0, s_2 \to 0$, $p(w_1(s_1), w_2(s_2)) = (t_1(s_1, s_2) w_1(s_1) + \hat{l}_1, t_2(s_1, s_2) w_2(s_2) + \hat{l}_2) \to p(w_1, w_2)$ as $s_1 \to 0, s_2 \to 0$ and hence $sign(t_i(s_1, s_2)) = sign(t_i)$,$|t_i(s_1, s_2)| > \frac{|t_i|}{2}$, for small $s_i > 0$, $i = 1, 2$. By the definition of p, $d_i \perp [w_i, L_i]$ so $d_i \perp w_i(s_1, s_2)$ and $d_i \perp p_i(w(s_1, s_2))$.

Now we have

$$
\begin{aligned}
& F(p_1(w_1(s_1), w_2(s_2)), p_2(w_1, w_2)) - F(p(w_1, w_2))) \\
= \; & \langle F_u(p(w_1, w_2)), p_1(w_1(s_1), w_2(s_2)) - p_1(w_1, w_2)\rangle \\
& + o(\|p_1(w_1(s_1), w_2(s_2)) - p_1(w_1, w_2)\|) \\
= \; & \langle F_u(p(w_1, w_2)), p_1(w_1(s_1), w_2(s_2))\rangle - \langle F_u(p(w_1, w_2)), p_1(w_1, w_2)\rangle \\
& + o(\|p_1(w_1(s_1), w_2(s_2)) - p_1(w_1, w_2)\|) \\
= \; & \langle F_u(p(w_1, w_2)), p_1(w_1(s_1), w_2(s_2))\rangle + o(\|p_1(w_1(s_1), w_2(s_2)) - p_1(w_1, w_2)\|) \\
= \; & \langle F_u(p(w_1, w_2)), w_1(s_1) \cdot t_1(s_1, s_2) + \hat{l}_1\rangle + o(\|p_1(w_1(s_1), w_2(s_2)) - p_1(w_1, w_2)\|) \\
= \; & \langle F_u(p(w_1, w_2)), \frac{w_1 - sign(t_1)s_1 d_1}{\|w_1 - sign(t_1)s_1 d_1\|} \cdot t_1(s_1, s_2)\rangle \\
& + o(\|p_1(w_1(s_1), w_2(s_2)) - p_1(w_1, w_2)\|) \\
= \; & \langle F_u(p(w_1, w_2)), \frac{w_1 - sign(t_1)s_1 d_1}{\|w_1 - sign(t_1)s_1 d_1\|} \cdot t_1(s_1, s_2)\rangle \\
& + o(\|p_1(w_1(s_1), w_2(s_2)) - p_1(w_1, w_2)\|) \\
= \; & -\frac{s_1 \cdot |t_1(s_1, s_2)|\|d_1\|^2}{\|w_1 - sign(t_1)s_1 d_1\|} + o(\|p_1(w_1(s_1), w_2(s_2)) - p_1(w_1, w_2)\|) \\
< \; & -\frac{s_1 |t_1| \cdot \|d_1\|^2}{2\|w_1 - sign(t_1)s_1 d_1\|} \quad \text{for } s_1 \text{ small} \\
< \; & -\frac{1}{4} s_2 \cdot |t_1|\|d_2\|^2 \quad \text{by Lemma 3.1.1.}
\end{aligned}
$$

By a similar argument we can get that

$$
\begin{aligned}
& G(p_1(w_1, w_2)), p_2(w_1(s_1), w_2(s_2))) - G(p(w_1, w_2))) \\
& < -\tfrac{1}{4} s_2 \cdot |t_2|\|d_2\|^2 \quad \text{for } s_2 \text{ small.}
\end{aligned}
$$

So we conclude $\exists s_0 > 0$ s.t. the statement is true. ■

Now we are ready to establish a local game-type characterization of multiple solutions to (1.15).

Theorem 3.1.2 *Suppose that F, G are in $\mathcal{C}^1(H, \mathbb{R})$, L is a closed subspace of H , $w = (w_1, w_2) \in S_{L^\perp}$, $p(w) = (p_1(w), p_2(w))$ is a joint orthogonal selection of $(F(u, v), G(u, v))$ at w. If*

(a) p is continuous at w;

(b) $dist(p_1(w), L_1) > 0$, $dist(p_2(w), L_2) > 0$;

(c)

$$(w_1, w_2) = arg \begin{cases} \min\limits_{\hat{w}_1 \in S_{L_1^\perp}} F(p(\hat{w}_1, \hat{w}_2)), \\ \min\limits_{\hat{w}_2 \in S_{L_2^\perp}} G(p(\hat{w}_1, \hat{w}_2)), \end{cases} \tag{3.5}$$

then $F_u(p(w)) = G_v(p(w)) = 0$.

Proof Suppose either $\|F_u(p(w))\| > 0$ or $\|G_v(p(w))\| > 0$. The we can apply Theorem 3.1.1 to get either (3.3) or (3.4), which violates the condition (c). So $F_u(p(w)) = G_v(p(w)) = 0$. ■

By Theorem 3.1.2, we can propose the following joint local min orthogonal method (JLMOM).

$$(w_1, w_2) = arg \begin{cases} \min\limits_{\hat{w}_1 \in S_{L_1^\perp}} F(p(\hat{w}_1, \hat{w}_2)), \\ \min\limits_{\hat{w}_2 \in S_{L_2^\perp}} G(p(\hat{w}_1, \hat{w}_2)). \end{cases} \tag{3.6}$$

This is a two-level method. The inner level computes a joint orthogonal selection s.t. $F_u(p(w_1, w_2)) = 0$ in L_1 and $G_v(p(w_1, w_2)) = 0$ in L_2. The outer level minimizes $F(p(w_1, w_2))$ with w_1 in $L_1^\perp$ and $G(p(w_1, w_2))$ with w_2 in $L_2^\perp$. So the result of the method satisfies $F_u(p(\hat{w}_1, \hat{w}_2)) = 0$ and $G_v(p(\hat{w}_1, \hat{w}_2)) = 0$ in H.

The original Palais-Smale(PS) is not applicable here because we do not have a variational form. However a certain compactness is needed for the convergence analysis of our algorithm. So we propose a modified (PS) condition.

Definition 3.1.3 *$(F(u,v), G(u,v)) \in \mathcal{C}^1(H_1 \times H_2, \mathbb{R}^2)$ is said to satisfy the joint Palais-Smale(JPS)condition if any sequence $\{(u^k, v^k)\} \subset (H_1 \times H_2)$ s.t.*

(a) $F(u^k, v^k)$ and $G(u^k, v^k)$ are bounded,

(b) $(F_u(u^k, v^k), G_v(u^k, v^k)) \to (0, 0)$,

has a convergent subsequence.

3.2 A Joint Local Min Orthogonal Algorithm

Now we propose our joint local min orthogonal algorithm based on the discussion in the previous section.

Step 0: Set a support $L = L_1 \times L_2$, select an initial guess $(w_1^0, w_2^0) \in S_{L^\perp}$ and set $k = 0$;

Step 1: Evaluate and denote $(u^k, v^k) \equiv p((w_1^k, w_2^k)) \equiv (t_1^k w_1^k + u_{L_1}^k, t_2^k w_2^k + v_{L_2}^k)$ from

$$F_u(u^k, v^k) \perp [L_1, w_1^k],\ G_v(u^k, v^k) \perp [L_2, w_2^k].$$

, where w_1^k, w_2^k are chosen s.t. $t_1^k > 0$ and $t_2^k > 0$(*Initial guess for evaluating p here is important, and we will discuss this later*);

Step 2: Evaluate and denote $d^k = (d_1^k, d_2^k) = (F_u(u^k, v^k), G_v(u^k, v^k))$;

Step 3: If $\|d^k\| < \varepsilon_0$, stop and output (u^k, v^k) otherwise do Step 4;

Step 4: Denote $w_1^k(s_1) = \frac{w_1^k - s_1 d_1^k}{\|w_1^k - s_1 d_1^k\|}$ $w_2^k(s_2) = \frac{w_2^k - s_2 d_2^k}{\|w_2^k - s_2 d_2^k\|}$.

Find maximum s_1^k and s_2^k of the form $\frac{1}{2^{m_k}}$, $m_k \in \mathbb{Z}^+$ from the step-size rule

$$F(p_1(w_1^k(s_1^k), w_2^k(s_2^k)), v^k) - F(u^k, v^k) \ < \ -\frac{s_1^k t_1^k}{4}\|d_1^k\|^2 \quad \text{if } d_1^k \neq 0, \tag{3.7}$$

$$G(u^k, p_2(w_1^k(s_1^k), w_2^k(s_2^k))) - G(u^k, v^k) \ < \ -\frac{s_2^k t_2^k}{4}\|d_2^k\|^2 \quad \text{if } d_2^k \neq 0, \tag{3.8}$$

$$F(u^k, p_2(w_1^k(s_1^k), w_2^k(s_2^k))) - F(u^k, v^k) + G(p_1(w_1^k(s_1^k), w_2^k(s_2^k)), v^k) - G(u^k, v^k) < \frac{C}{k^{1+\sigma}} \text{ for some } C, \sigma > 0, \tag{3.9}$$

$$\frac{1}{\kappa} < \frac{\|d_1^k(s^k)\|}{\|d_2^l(s^k)\|} < \kappa, \quad \text{for some } \kappa > 0; \tag{3.10}$$

where $p(w_1^k(s_1^k), w_2^k(s_2^k)) = (p_1(w_1^k(s_1^k), w_2^k(s_2^k)), p_2(w_1^k(s_1^k), w_2^k(s_2^k)))$ and $d^k(s^k) = (d_1^k(s^k), d_2^k(s^k)) = (F_u(p(w^k(s^k))), G_v(p(w^k(s^k))))$.

Step 5: Set $w_1^{k+1} = w_1^k(s^k)$, $w_2^{k+1} = w_2^k(s^k)$, $(u^{k+1}, v^{k+1}) \equiv p((w_1^k(s^k), w_2^k(s^k))$ and $k = k + 1$, Goto Step 2.

The algorithm can be stated in the following flow chart, Fig 3.1

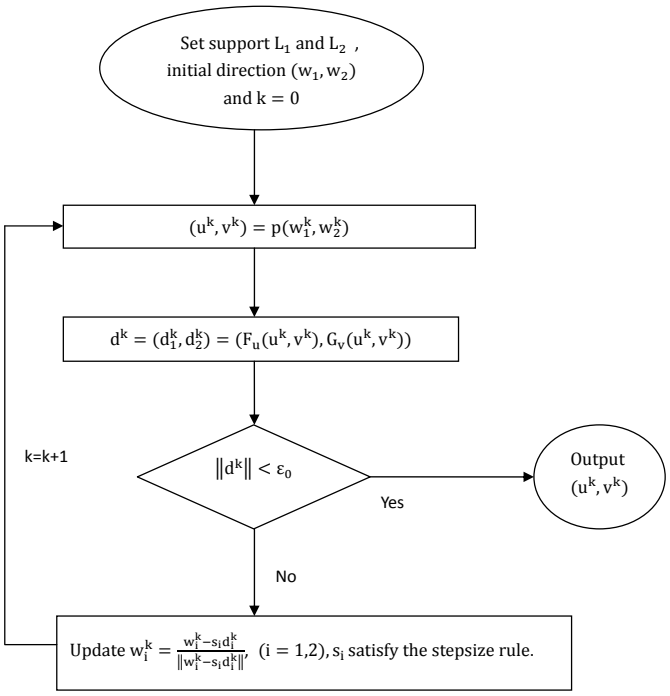

Fig. 3.1. The flow chart of the joint local min orthogonal algorithm.

3.2.1 A derivation of the step size rule

Based on Theorem 3.1.1 we get the following step size rule,

$$F(p_1(w^{k+1}), v^k) - F(u^k, v^k) \quad < -\tfrac{s_1^k \alpha}{2} \|d_1^k\|^2 \quad \text{if } d_1^k \neq 0, \tag{3.11}$$

$$G(u^k, p_2(w^{k+1})) - G(u^k, v^k) \quad < -\tfrac{s_2^k \alpha}{4} \|d_2^k\|^2 \quad \text{if } d_2^k \neq 0. \tag{3.12}$$

It is based on the condition that both $d_1^k \neq 0$, $d_2^k \neq 0$, and this can always be done by coordinating the convergent speed of the two parts, e.g. in our algorithm , besides a proper initial guess we also add another ratio condition for the step-size that

$$\frac{1}{\kappa} < \frac{\|d_1^k(s^k)\|}{\|d_2^l(s^k)\|} < \kappa \tag{3.13}$$

for some $\kappa > 0$ where

$$d^k(s^k) = (d_1^k(s^k), d_2^k(s^k)) = (F_u(p(w^k(s^k))), G_v(p(w^k(s^k)))).$$

That is when the norm of the gradient of one part is too small relative to the other part, the algorithm then slows down the progress of that part. And the constraint will not hurt the convergence of the algorithm, because it only balances the progressive speed of both part, but the range of the search has not been changed.

Unlike the cooperative variational case, besides the normal step-size-rule, we introduce new criteria that require, for some fixed $\sigma > 0$

$$F(p_1(w_1^k, w_2^k), p_2(w_1^k(s_1^k), w_2^k(s_2^k))) - F(p(w_1^k, w_2^k)) \quad < \tfrac{C}{k^{1+\sigma}}, \tag{3.14}$$

$$G(p_1(w_1^k, w_2^k), p_2(w_1^k(s_1^k), w_2^k(s_2^k))) - G(p(w_1^k, w_2^k)) \quad < \tfrac{C}{k^{1+\sigma}} \tag{3.15}$$

to control $F_v(p(w^k))$ and $G_u(p(w^k))$, which are needed for our convergence analysis. In computation, if we set C to be the number of maximal iteration allowed, the conditions will always be hold.

3.2.2 A revision of the energy function

Because for any functionals $\hat{f}(v)$ of v and $\hat{g}(u)$ of u

$$\begin{cases} \bar{F}_u(u) + W_u^1(u,v) + \hat{f}_u(v) = \bar{F}_u(u) + W_u^1(u,v) = 0, \\ \bar{G}_v(v) + W_v^2(u,v) + \hat{g}_v(u) = \bar{G}_v(v) + W_v^2(u,v) = 0, \end{cases} \tag{3.16}$$

we can slightly revise our energy functionals as follows

$$\begin{cases} F(u,v) = \bar{F}(u) + W^1(u,v) + \hat{f}(v), \\ G(u,v) = \bar{G}(v) + W_2(u,v) + \hat{g}(u) \end{cases} \tag{3.17}$$

for some auxiliary functionals $\hat{f}(v)$, $\hat{g}(u)$, without changing the solutions of our system. As stated in the step-size rule, we try to control the terms

$$\begin{cases} F(p_1(w_1,w_2)), p_2(w_1(s_1), w_2(s_2))) - F(p(w_1,w_2))), \\ G(p_1(w_1(s_1), w_2(s_2)), p_2(w_1,w_2)) - G(p(w_1,w_2))), \end{cases} \tag{3.18}$$

which implies that the following two conditions are desired.

$$\begin{cases} \langle F_v(p(w_1,w_2)), G_u(p(w_1,w_2))\rangle > 0, \\ \langle F_u(p(w_1,w_2)), G_v(p(w_1,w_2))\rangle > 0. \end{cases} \tag{3.19}$$

For variational cases, the best choice of the auxiliary functionals is simply to create a variational form $J(u,v) = F(u,v) \pm kG(u,v)$. For non-variational cases, in general it is impossible to satisfying the two inequalities (3.19), we want to get as close as possible. when $F(u,v)$ has the mountain pass structure in u as v fixed and $G(u,v)$ has the mountain-pass structure in v as u fixed, we choose $\hat{f}(v) = \bar{G}(v)$ and $\hat{g}(u) = \bar{F}(u)$.

3.2.3 Choosing initial guess for the joint orthogonal selection

In implementation, we write the joint orthogonal selection as , where t_1, t_2, c_{1_i} are unknown coefficients. To compute these coefficients, we need solve a large non-linear algebraic system of equations.

$$
\begin{cases}
\langle F_u(p(w_1,w_2)), w_1\rangle = & 0, \\
\langle F_u(p(w_1,w_2)), l_{1_1}\rangle = & 0, \\
\qquad\qquad\qquad\qquad \vdots & \\
\langle F_u(p(w_1,w_2)), l_{1_n}\rangle = & 0, \\
\langle G_v(p(w_1,w_2)), w_2\rangle = & 0, \\
\langle G_v(p(w_1,w_2)), l_{2_1}\rangle = & 0, \\
\qquad\qquad\qquad\qquad \vdots & \\
\langle G_v(p(w_1,w_2)), l_{2_m}\rangle = & 0,
\end{cases}
\tag{3.20}
$$

where $L_1 = span\{l_{1_1}, .., l_{1_n}\}$ and $L_2 = span\{l_{2_1}, .., l_{2_m}\}$.

Numerically, we use Newton's method to solve the algebraic system, which requires a good initial guess. For single equation or cooperative cases, in which $p(w)$ is actually a local maximum in a subspace, the search direction of Newton's method is given. In the non-variational system case, $p(w_1, w_2)$ is no longer an extreme in a subspace, so a more sophisticated initial guess of Newton's method has to be selected. For example, when $F(u, v)$ has mountain pass structure in u as v fixed and $G(u, v)$ has mountain-pass structure in v as u fixed, we first compute

$$
\begin{cases}
u^* = arg \max\limits_{u\in[w_1,L_1]} \bar{F}(u), \\
v^* = arg \max\limits_{v\in[w_2,L_2]} \bar{G}(v),
\end{cases}
\tag{3.21}
$$

and then use (u^*, v^*) as an initial guess for Newton's method to solve the algebraic system. Our numerical experience shows that this is very important for the first several iterations when the approximation is still far away from its accurate solution, while using the approximation of the previous iteration as an initial guess performs poorly.

3.2.4 Convergence of the algorithm

Now we can give the convergence of the algorithm in functional analysis. The convergence based on error analysis is not yet available, however in our algorithm the error is not accumulative in the iterations, i.e., the result of each iteration can be regarded as a new initial guess for the next iteration. To maintain the accuracy of our algorithm the tolerance that we choose for Newton's method and finite element method is much smaller than that of our algorithm.

Theorem 3.2.1 *Assume F and G satisfy JPS condition. Let $\{(w_1^k, w_2^k)\}$ be the sequence generated by our algorithm satisfying*

(a) $p(\cdot,\cdot)$, the joint orthogonal selection, is continuous at (w_1^k, w_2^k),

(b) $dist(p_1(w_1^k, w_2^k), L_1) > \alpha > 0$, $dist(p_2(w_1^k, w_2^k), L_2) > \alpha > 0$,

(c) $F(p(w_1^k, w_2^k))$ and $G(p(w_1^k, w_2^k))$ are bounded from below.

Then $p(w_1^k, w_2^k) \to p(w_1^*, w_2^*)$ with $F_u(p(w_1^*, w_2^*)) = 0$, and $G_v(p(w_1^*, w_2^*)) = 0$.

Proof First, from the algorithm we see that

$$\begin{aligned} & F(p(w^{k+1})) - F(p(w^k)) \\ = \; & \langle F_u(p(w^k)), p_1(w^{k+1}) - p_1(w^k)\rangle + \langle F_v(p(w^k)), p_2(w^{k+1}) - p_2(w^k)\rangle \\ & + o(\|p_1(w^{k+1}) - p_1(w^k)\|) + o(\|p_2(w^{k+1}) - p_2(w^k)\|), \end{aligned} \tag{3.22}$$

$$
\begin{aligned}
& F(p_1(w^{k+1}), p_2(w^k)) - F(p(w^k)) \\
(3.23) \qquad = \; & \langle F_u(p(w^k)), p_1(w^{k+1}) - p_1(w^k)\rangle + o(\|p_1(w^{k+1}) - p_1(w^k)\|), \\
& F(p_1(w^k), p_2(w^{k+1})) - F(p(w^k)) \\
(3.24) \qquad = \; & \langle F_v(p(w^k)), p_2(w^{k+1}) - p_2(w^k)\rangle + o(\|p_2(w^{k+1}) - p_2(w^k)\|).
\end{aligned}
$$

Comparing (3.22) with (3.23) and (3.24), we get

$$
\begin{aligned}
& F(p(w^{k+1})) - F(p(w^k)) \\
= \; & F(p_1(w^{k+1}), p_2(w^k)) - F(p(w^k)) + F(p_1(w^k), p_2(w^{k+1})) - F(p(w^k)) \\
(3.25) \qquad & + o(\|p_1(w^{k+1}) - p_1(w^k)\|) + o(\|p_2(w^{k+1}) - p_2(w^k)\|).
\end{aligned}
$$

Similarly we can get an estimate in $G(u, v)$

$$
\begin{aligned}
& G(p(w^{k+1})) - G(p(w^k)) \\
= \; & G(p_1(w^{k+1}), p(w^k)) - G(p(w^k)) + G(p_1(w^k), p_2(w^{k+1})) - G(p(w^k)) \\
(3.26) \qquad & + o(\|p_1(w^{k+1}) - p_1(w^k)\|) + o(\|p_2(w^{k+1}) - p_2(w^k)\|).
\end{aligned}
$$

From (3.25),(3.26) and the stepsize rule, we get

$$
\begin{aligned}
(3.27) \qquad & F(p(w^{k+1})) - F(p(w^k)) + G(p(w^{k+1})) - G(p(w^k)) \\
= \; & F(p_1(w^{k+1}), p_2(w^k)) - F(p(w^k)) + G(p_1(w^k), p_2(w^{k+1})) - G(p(w^k)) \\
& + F(p_1(w^k), p_2(w^{k+1})) - F(p(w^k)) + G(p_1(w^{k+1}), p(w^k)) - G(p(w^k)) \\
& + o(\|p_1(w^{k+1}) - p_1(w^k)\|) + o(\|p_2(w^{k+1}) - p_2(w^k)\|) \\
< \; & -\frac{s_1^k \alpha}{2}\|d_1^k\|^2 - \frac{s_2^k \alpha}{2}\|d_2^k\|^2 + \frac{C}{k^{1+\sigma}}.
\end{aligned}
$$

Take the summation of the two sides of (3.27) for $k = 1, 2, ...$, we get

$$\begin{aligned} -\infty &< \lim_{k\to\infty}[F(p(w^k)) - F(p(w^1))] + \lim_{k\to\infty}[G(p(w^k)) - G(p(w^1))] \\ &= \sum_{k=1}^{\infty}\left[F(p(w^{k+1})) - F(p(w^k)) + G(p(w^{k+1})) - G(p(w^k))\right] \\ &< -\frac{\alpha}{2}\sum_{k=1}^{\infty}(s_1^k\|d_1^k\|^2 + s_2^k\|d_2^k\|^2) + C\sum_{k=1}^{\infty}\frac{1}{k^{1+\sigma}} \\ &< -\frac{\alpha}{4}\sum_{k=1}^{\infty}\|w_1^{k+1} - w_1^k\|\|d_1^k\| - \frac{\alpha}{4}\sum_{k=1}^{\infty}\|w_2^{k+1} - w_2^k\|\|d_2^k\| + C\sum_{k=1}^{\infty}\frac{1}{k^{1+\sigma}}. \end{aligned}$$

This implies that

$$\begin{aligned} &\frac{\alpha}{4}\sum_{k=1}^{\infty}\|w_1^{k+1} - w_1^k\|\|d_1^k\| + \frac{\alpha}{4}\sum_{k=1}^{\infty}\|w_2^{k+1} - w_2^k\|\|d_2^k\| \\ &< \frac{\alpha}{2}\sum_{k=1}^{\infty}(s_1^k\|d_1^k\|^2 + s_2^k\|d_2^k\|^2) < \infty. \end{aligned} \tag{3.28}$$

Now suppose $\{d^k\}$ does not have any subsequence that goes to $(0, 0)$. Without loss of generality, we may assume that $\|d^k\| > \delta > 0$ for all $k = 1, 2, ...$

By $\frac{1}{\kappa} < \frac{\|d_1^k\|}{\|d_2^k\|} < \kappa$, for some $\kappa > 0$, we get $\|d_1^k\| > \frac{\delta}{\sqrt{1+\kappa^2}}$, $\|d_2^k\| > \frac{\delta}{\sqrt{1+\kappa^2}}$.

Then we have

$$\begin{aligned} \frac{\delta}{\sqrt{1+\kappa^2}}\sum_{k=1}^{\infty}\|w_1^{k+1} - w_1^k\| &< \sum_{k=1}^{\infty}\|w_1^{k+1} - w_1^k\|\|d_1^k\| < \infty, \\ \frac{\delta}{\sqrt{1+\kappa^2}}\sum_{k=1}^{\infty}\|w_2^{k+1} - w_2^k\| &< \sum_{k=1}^{\infty}\|w_2^{k+1} - w_2^k\|\|d_2^k\| < \infty, \\ \frac{\delta}{\sqrt{1+\kappa^2}}\sum_{k=1}^{\infty}s_1^k &< \sum_{k=1}^{\infty}s_1^k\|d_1^k\|^2 < \infty, \\ \frac{\delta}{\sqrt{1+\kappa^2}}\sum_{k=1}^{\infty}s_2^k &< \sum_{k=1}^{\infty}s_2^k\|d_2^k\|^2 < \infty, \end{aligned}$$

which imply that $\{w^k\}$ is a Cauchy sequence in H and $s^k \to 0$. So $w^k \to w^* \in H$ with $\|(F_u(p(w^*), G_v(p(w^*))\| \geq \delta$.

Then by Theorem 3.1.1, in a small neighborhood of $w^*, \mathcal{N}(w^*) = \mathcal{N}(w_1^*) \oplus \mathcal{N}(w_2^*)$, there exists $s(w^*) = (s_1(w^*), s_2(w^*))$ with $s_1(w^*) > \eta > 0, s_2(w^*) > \eta > 0$ that satisfies the step-size condition for all $w^k \subset \mathcal{N}(w^*)$. But this contradicts with that $s^k \to 0$ So $\{F_u(p(w^k)), G_v(p(w^k))\} = \{d^k\}$ has a subsequence $\{d^{k_i}\}$ converging to $(0, 0)$. By JPS condition, $\{p(w^{k_i}\}$ has a subsequence, denoted by $\{p(w^{k_i}\}$ again, converging to $p^* = (p_1^*, p_2^*) \in H$ with $p_1^* \notin L_1$ and $p_2^* \notin L_2$. Next we prove that there is $w^* = (w_1^*, w_2^*) \in S_{L_1^\perp} \oplus S_{L_2^\perp}$ s.t. $w^{k_i} \to w^*$ and $p(w^*) = p^*$. Denote $p_j^* = w_j' + w_{L_j}'$ for some $0 \neq w_j' \in L_j^\perp$ and $w_{L_j}' \in L_j, j = 1, 2$. Then

$$p(w^{k_i}) = (t_1^{k_i} w_1^{k_i} + w_{L_1}^{k_i}, t_2^{k_i} w_2^{k_i} + w_{L_2}^{k_i}) \to p^*$$

implies for $j = 1, 2$, we have $t_j^{k_i} w_j^{k_i} \to w_j' \neq 0$ or $t_j^{k_i} \to \|w_j'\| \neq 0$ since $\|w_j^{k_i}\| = 1$. Thus $w_j^{k_i} \to w_j^* = \frac{w_j'}{\|w_j'\|}$. Denote $w^* = (w_1^*, w_2^*) \in S_{L_1^\perp} \oplus S_{L_2^\perp}$. Thus $w^{k_i} \to w^*$. Then by the continuity of p, we proved

$$p(w^{k_i}) \to p(w^*) = p^*.$$

To prove the full sequence convergence, we apply the inequality (3.2) with $w^{k_i} = (w_1^{k_i}, w_2^{k_i})$, $w_j^{k_i+1} = \frac{w_j^{k_i} - s_j^{k_i} d_j^{k_i}}{\|w_j^{k_i} - s_j^{k_i} d_j^{k_i}\|}, j = 1, 2$. Thus

$$\|w_j^{k_i+1} - w_j^{k_i}\| \leq \frac{2|s_j^{k_i}| \|d_j^{k_i}\|}{\|w_j^{k_i} + s_j^{k_i} d_j^{k_i}\|} \to 0,$$

since $\|w_j^{k_i}\| = 1, |s_j^{k_i}|$ is bounded by the algorithm and the term $\frac{2|s_j^{k_i}|}{\|w_j^{k_i} + s_j^{k_i} d_j^{k_i}\|}$ is also bounded. Hence

$$w^{k_i+1} \to w^*.$$

Then we can merge the two sequences $\{w^{k_i}\}$ and $\{w^{k_i+1}\}$ together to form a larger convergent subsequence. Carrying on this process repeatedly. Each time we obtain a larger subsequence converging to w^*. So we have a monotone increasing sequence of subsequences converging to w^*. This sequence has an upper bound, i.e., the whole sequence. By Zorn's lemma, there must be a maximum subsequence converging to w^*. It must be the whole sequence, since otherwise, a larger subsequence converging to w^* can always be obtained by the above process, which will violate the maximum statement by Zorn's lemma. Thus we obtain that

$$w^k \to w^* \quad \text{and} \quad p(w^k) \to w^* = p(w^*).$$

■

3.3 Numerical Example

The model we computed as an example is,

$$\begin{cases} -\Delta u + \lambda_1 u + \mu_1 u^3 + \beta_1 u v^2 + \theta_1 |u| u v^2 = 0, \\ -\Delta v + \lambda_2 v + \mu_2 v^3 + \beta_2 u^2 v + \theta_2 u^2 |v| v = 0 \end{cases} \tag{3.29}$$

with $\frac{\beta_1}{\beta_2} \neq \frac{\theta_1}{\theta_2}$. This is a non-variational system of the form (1.16), with

$$\begin{cases} F(u,v) = \frac{1}{2}\nabla|u|^2 + \frac{1}{2}\lambda_1 u^2 + \frac{1}{4}\mu_1 u^4 + \frac{1}{2}\beta_1 u^2 v^2 + \frac{1}{3}\theta_1 |u| u^2 v^2, \\ G(u,v) = \frac{1}{2}\nabla|v|^2 + \frac{1}{2}\lambda_2 v^2 + \frac{1}{4}\mu_2 v^4 + \frac{1}{2}\beta_2 u^2 v^2 + \frac{1}{3}\theta_2 u^2 |v| v^2. \end{cases} \tag{3.30}$$

The system is a modification of the well-known Gross-Pitaevskii system in Bose Einstein condensate, so mathematically we can expect some similar solutions to justify our algorithm and computation. For the example in Fig. 3.2, we take $\lambda_1 =$

-0.9; $\lambda_2 = -1.1$; $\mu_1 = 3$; $\mu_2 = 3$; $\beta_1 = 1$; $\beta_2 = 1.1$; $\theta_1 = 0.3$; $\theta_2 = 0.2$. The tolerance is 10^{-3} and the domain is $(-0.5, 0.5)^2$.

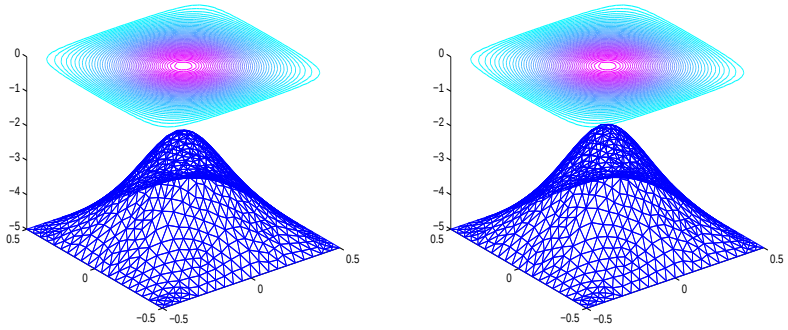

Fist solution set

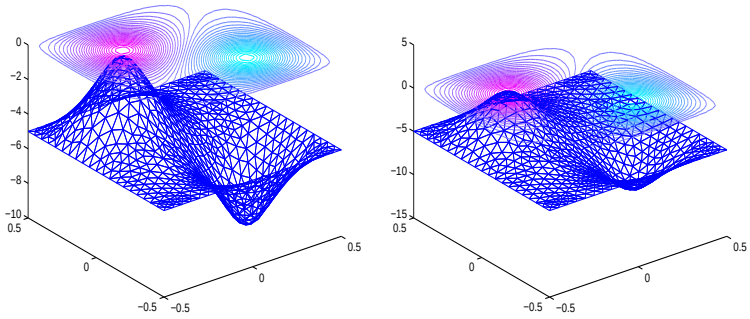

Second solution set

Fig. 3.2. Numerical solutions of the system (3.29).

4. CONCLUSION

In this thesis, we have discussed two types of non-variational nonlinear PDE problems, a semi-linear elliptic eigen solution problem and a semi-linear elliptic system without a common variational form. Numerical methods have been developed for both problems to compute their multiple solutions in an order and their mathematical justifications have been established.

For the semi-linear elliptic eigen solution problem, we introduced a new constraint on the variational energy level. With this new approach, by the inverse functional theorem, we can define the eigenvalue λ implicitly as a functional of eigenfunction u, and the original eigen solution problem is then equivalent to find the critical points of the functional $\lambda(u)$. The advantage of this approach is that we are now possible to find the multiple eigen-solutions in the order of their eigenvalues and furthermore in Neumann boundary condition cases, it enables us to identify bifurcations and find different solution branches. We applied the local min-max method to numerically compute the solutions of focusing type eigen solution problem. The numerical results strongly support our analysis. For defocusing type eigen solution problem, we developed an orthogonal subspace minimization method to compute the solutions with certain symmetry. Many numerical examples have been carried out to test the algorithm.

For the non-variational semi-linear elliptic system, a joint local min orthogonal method has been designed. Under certain condition, the convergence of the algorithm has been proved and a non-variational system has been numerically tested for the algorithm.

REFERENCES

[1] W. Bao and Q. Du, Computing the ground state solution of Bose-Einstein condensates by a normalized gradient flow, *SIAM J. Sci. Comp.* **25**(2004) 1674-1697.

[2] T. Bodurov, Derivation of the nonlinear Schrodinger equation from first principle, *Annales de la Fondation Louis de Broglie* **30**(2005) 1-10.

[3] A. Castro, J. Cossio and J. Neuberger, A sign-changing solution for a perlinear Direichlet problem, *Rocky Mountain Jounal of Mathematics*, **27**(1997), 1041-1053.

[4] S.-L. Chang and C.-S. Chien, Computing multiple peak solutions for Bose-Einstein condensates in optical lattics, *Comp. Phy. Comm.* **180**(2009) 926-947.

[5] G. Chen, W.M. Ni and J. Zhou, Algorithms and visualization for solutions of nonlinear elliptic equation, Part I: Dirichlet Problem, *Int. J. Bifur. Chaos*, **7**(2000) 1565-1612.

[6] M. Chipot (editor), *Handbook of Differential Equations: Stationary Partial Differential Equations*, Elsevier, Oxford, 2008.

[7] S. N. Chow and R. Lauterbach, A bifurcation theorem for critical points of variational problems, *Nonlinear Anal.*, **12**(1988) 51-61.

[8] Y. Deng, G. Chen, W. Ni, and J. Zhou, Boundary element monotone iteration scheme for semilinear elliptic partial differential equations, *Math. Comp.*,**65**(1996) 943-982.

[9] Z. Ding, D. Costa and G. Chen, A high linking method for sign changing solutions for semilinear elliptic equation. *Nonlinear Anal.*, **38**(1999) 151-172.

[10] C. Gui, Multipeak solutions for a semilinear Neumann problem, *Duke Math. J.*, **84**(1996) 739-769.

[11] Y. Li and J. Zhou, A minimax method for finding multiple critical points and its applications to semilinear elliptic PDEs, *SIAM Sci. Comp.*, **23**(2001), 840-865.

[12] Y. Li and J. Zhou, Convergence results of a local minimax method for finding multiple critical points, *SIAM Sci. Comp.*, **24**(2002) 865-885.

[13] C. S. Lin, W. M. Ni, and I. Takagi, Large amplitude stationary solutions to a chemotaxis system, *J. Diff. Eqns.*, **72**(1988) 1-27.

[14] T.I. Lakoba and J. Yang, A generalized Petviashvili iteration method for scalar and vector Hamiltonian equations with arbitrary form of nonlinearity *J. Comp. Phys.*, **226**(2007) 1668-1692.

[15] T.I. Lakoba and J. Yang, A mode elimination technique to improve convergence of iteration methods for finding solitary waves, *J. Comp. Phys.*, **226**(2007) 1693-1709.

[16] M. Morse, The Calculus of Variations in the Large. *AMS Colloquium Publication* **18**(1934).

[17] Y. Matsumoto, *An Introduction to Morse Theory*, AMS, Providence, 2002.

[18] M.Z. Nashed and X. Chen, Convergence of Newton like method for singular operator equations using outer inverse, *Numer. Math.*, **66**(1993), 235-257.

[19] J. Neuberger and J. Swift, Newton's method and Morse index for semilinear elliptic PDEs, *Int. J. Bifur. Chaos*, **11**(2001), 801-820.

[20] W. M. Ni and I. Takagi, On the Neumann probem for some semilinear elliptic equations and systems of activator-inhibitor type, *Trans. Amer. Math. Soc.*, **297**(1986) 351-368.

[21] P.H. Rabinowitz, Critical point theory and applications to differential equations: a survey. Topological Nonlinear Analysis, 464-513, *Progr. Nonlinear Differential Equations Appl.*, 15, Birkhäuser Boston, Boston, MA, (1995).

[22] P. Rabinowitz, Minimax Method in Critical Point Theory with Applications to Differential Equations, *CBMS Regional Conf. Series in Math.,* No. 65, AMS, Providence, 1986.

[23] M. Schechter, *Linking Methods in Critical Point Theory*, Birkhauser, Boston, 1999.

[24] E. W. C. Van Groesen and T. Nijmegen, Continuation of solutions of constrained extremum problems and nonlinear eigenvalue problems, *Math. Model.*, **1**(1980) 255-270.

[25] Z.Q. Wang and J. Zhou, An efficient and stable method for computing multiple saddle points with symmetries, *SIAM J. Num. Anal.*, **43**(2005) 891-907.

[26] Z.Q. Wang and J. Zhou, A Local Minimax-Newton Method for Finding Critical Points with Symmetries, *SIAM J. Num. Anal.*, **42**(2004) 1745-1759.

[27] C. Wang and J. Zhou Solving Nonlinear Differential Eigen Problems By An Implicit Minimax Method ,*Submitted*.

[28] C. Wang and J. Zhou An Orthogonal Subspace Minimization Method for Finding Multiple Solutions to Defocusing Schrodinger Equation with Symmetries ,*Revising*

[29] T. Watanabe, K. Nishikawa, Y. Kishimoto and H. Hojo, Numerical method for nonlinear eigenvalue problems, *Physica Scripta.*, **T2/1**(1982) 142-146.

[30] M Willem, *Minimax Theorems*, Birkhauser, Boston, (1996).

[31] J. Yang, Newton-conjugate-gradient methods for solitary wave computations, *J. Comp. Phys.* **228**(2009) 7007-7024.

[32] J. Yang and T.I. Lakoba, Accelerated Imaginary-time Evolution Methods for the Computation of Solitary Waves, *Stud. Appl. Math.* **120**(2008) 265-292.

[33] X. Yao and J. Zhou, A minimax method for finding multiple critical points in Banach spaces and its application to quasilinear elliptic PDE, *SIAM J. Sci. Comp.*, **26**(2005) 1796-1809.

[34] X. Yao and J. Zhou, Numerical methods for computing nonlinear eigenpairs. Part I. iso-homogenous cases, *SIAM J. Sci. Comp.*,**29**(2007) 1355-1374.

[35] X. Yao and J. Zhou, Numerical methods for computing nonlinear eigenpairs. Part II. non iso-homogenous cases, *SIAM J. Sci. Comp.*, **30**(2008) 937-956.

[36] E. Zeidler, Ljusternik-Schnirelman theory on general level sets, *Math. Nachr.*, **129**(1986) 238-259.

[37] J. Zhou, A local min-orthogonal method for finding multiple saddle points, *J. Math. Anal. Appl.*, **291**(2004) 66-81.

[38] J. Zhou, Instability analysis of saddle points by a local minimax method, *Math. Comp.*, **74**(2005) 1391-1411.

[39] J. Zhou, Global sequence convergence of a a local minimax method for finding multiple solutions in Banach spaces, *Num. Func. Anal. Optim.*, **32**(2011) 1365-1380.

[40] X. Chen and J. Zhou , A Local Min-Max-Orthogonal Method for Finding Multiple Solutions to Noncooperative Elliptic Systems",(pdf version) ,*Math. Comp.*, **79**(2010) 2213-2236.

[41] X. Chen and J. Zhou, A Local Min-Orthogonal Method for Multiple Solutions of Strongly Coupled Elliptic Systems", *Discrete and Continuous Dynamical Systems*, Supplement (2009) 151-160.

[42] X. Chen, X. Yao and J. Zhou, A Numerical Method for Finding Multiple Coexisting Solutions to Nonlinear Cooperative Systems, *Applied Numerical Mathematics* **58**(2008), pp. 1614-1627.

VITA

Name: Changchun Wang

Address : Department of Mathematics

Texas A&M University

College Station, TX 77843-3368

Phone: 979-739-1787

Email: cwang@math.tamu.edu

Education

May 2012, Texas A&M University, Ph.D. in Applied Math.
Thesis : On theory and numerical methods for finding multiple solutions of nonlinear partial differential equations(PDEs). Advisor: Jianxin Zhou.
July 2006, Shanghai University, Shanghai, China M.S. in Computational Math,
Thesis : On computation of multi-component flow. Advisor : De-Kang Mao.
July 2003, Shanghai University, Shanghai, China B.S. in Information and Computational Science, Thesis : Protein folding structure prediction.

Publications and Preprints

C.Wang and J. Zhou, Orthogonal Subspace Minimization Method for Finding Multiple Solutions to Defocusing Schrodinger Equation with Symmetries ,*Numerical Methods for Partial Differential Equations.* (Revising)
C.Wang and J. Zhou, Solving Nonlinear Differential Eigen Problems By An Implicit Minimax Method , *Mathematics of Computation.* (Submitted)
C.Wang and J. Zhou, Numerical methods for computing multiple solution of nonlinear PDE system without variational structure. (In preparation)
C.Wang and De-Kang Mao, Multi-component Flow Calculations, Communication on Applied Mathematics and Computation, 2006 Vol.20(2) Page 109-112 *(Chinese)*